
PerSim: Data-Efficient Offline Reinforcement Learning with Heterogeneous Agents via Personalized Simulators

Anish Agarwal¹ Abdullah Alomar¹ Varkey Alumootil¹ Devavrat Shah¹ Dennis Shen¹ Zhi Xu¹ Cindy Yang¹

Abstract

We consider offline reinforcement learning (RL) with heterogeneous agents under severe data scarcity, i.e., we only observe a single historical trajectory for every agent under an unknown, potentially sub-optimal policy. We find that the performance of state-of-the-art offline and model-based RL methods degrade significantly given such limited data availability, even for commonly perceived “solved” benchmark settings such as “MountainCar” and “CartPole”. To address this challenge, we propose a model-based offline RL approach, called PerSim, where we first learn a personalized simulator for each agent by collectively using the historical trajectories across all agents prior to learning a policy. We do so by positing that the transition dynamics across agents can be represented as a latent function of latent factors associated with agents, states, and actions; subsequently, we theoretically establish that this function is well-approximated by a “low-rank” decomposition of separable agent, state, and action latent functions. This representation suggests a simple, regularized neural network architecture to effectively learn the transition dynamics per agent, even with scarce, offline data. We perform extensive experiments across several benchmark environments and RL methods. The consistent improvement of our approach, measured in terms of state dynamics prediction and eventual reward, confirms the efficacy of our framework in leveraging limited historical data to simultaneously learn personalized policies across agents.

1. Introduction

Reinforcement learning (RL) coupled with expressive deep neural networks has now become a generic yet powerful solution for learning complex decision-making policies for an agent of interest; it provides the key algorithmic foundation underpinning recent successes such as game

solving (Mnih et al., 2015; Silver et al., 2017b;a) and robotics (Levine et al., 2016; Kalashnikov et al., 2018). However, many state-of-the-art RL methods are data hungry and require the ability to query samples at will, which is infeasible for numerous settings such as healthcare, autonomous driving, and socio-economic systems. As a result, there has been a rapidly growing literature on “offline RL” (Levine et al., 2020; Kumar et al., 2019; Liu et al., 2020; Fujimoto et al., 2019), which focuses on leveraging existing datasets to learn decision-making policies.

Within offline RL, we consider a regime of *severe data scarcity*: there are multiple agents and for each agent, we only observe a single historical trajectory generated under an unknown, potentially sub-optimal policy; further, the agents are *heterogeneous*, i.e., each agent has unique state transition dynamics. Importantly, the characteristics of the agents that make their transition dynamics heterogeneous are *latent*. Using such limited offline data to *simultaneously* learn a good “personalized” policy for each agent is a challenging setting that has received limited attention in the literature. Below, we use a prevalent example from healthcare to motivate and argue that tackling such a challenge is an important and necessary step towards building personalized decision-making engines via RL in a variety of important applications.

A Motivating Example. Consider a pre-existing clinical dataset of patients (agents). Our goal is to design a personalized treatment plan (policy) for each patient moving forward. Notable challenges include the following: First, each patient only provides a single trajectory of their medical history. Second, each patient is heterogeneous in that s/he may have a varied response for a given treatment under similar medical conditions; further, the underlying reason for this heterogeneous response across patients is likely unknown and thus not recorded in the dataset. Third, in the absence of an accurate personalized “forecasting” model for a patient’s medical outcome given a treatment plan, the treatment assigned is likely to be sub-optimal. This is particularly true for complicated medical conditions like T-Cell Lymphoma. We aim to address the challenges laid out above (offline scarce data, heterogeneity, and sub-optimal policies) so as to develop a personalized “forecasting” model for each patient under any given treatment plan. Doing so will then naturally enable ideal personalized treatment policies for each patient. *Key question.* Tackling a scenario like the one described above in a principled manner is the focus of this work. In

¹ Massachusetts Institutes of Technology, Cambridge, MA, USA. Correspondence to: Abdullah Alomar <aalomar@mit.edu>.

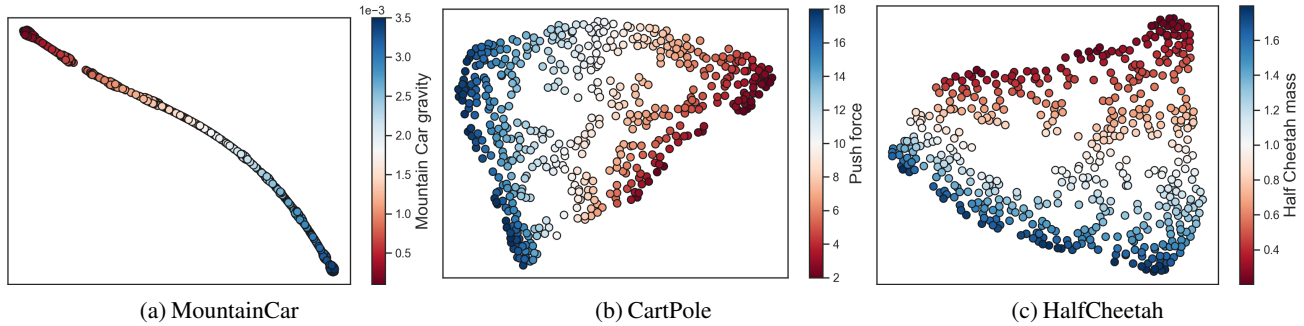


Figure 1. t-SNE visualization of the learned latent factors for the 500 heterogeneous agents. Colors indicate the value of the modified parameters in each environment (e.g., gravity in MountainCar). There is an informative low-dimensional manifold induced by the latent factors, and there is a natural direction on the manifold along which the parameters that characterizes the heterogeneity varies continuously and smoothly.

particular, we seek to answer the following question:

“Can we leverage scarce, offline data collected across heterogeneous agents under unknown, sub-optimal policies to learn a personalized policy for each agent?”

Our Contributions. As the main contribution of this work, we answer this question in the affirmative by developing a structured framework to tackle this challenging yet meaningful setting. Next, we summarize the main methodological, theoretical, algorithmic, and experimental contributions in our proposed framework.

Methodological — personalized simulators. We propose a novel methodological framework, PerSim, to learn a policy given the data availability described above. Taking inspiration from the model-based RL literature, our approach is to first build a personalized simulator for each agent. Specifically, we use the offline data collectively available across heterogeneous agents to learn the unique transition dynamics for each agent. We do this *without* requiring access to the covariates or features that drive the heterogeneity amongst the agents. Having constructed a personalized simulator, we then learn a personalized decision-making policy separately for each agent by simply using online model predictive control (MPC) (Garcia et al., 1989; Camacho & Alba, 2013).

Theoretical — learning across agents. As alluded to earlier, the challenge in building a personalized simulator for each agent is that we only have access to a single offline trajectory for any given agent. Hence, each agent likely explores a very small subset of the entire state-action space. However, by viewing the trajectories across the multitude of agents collectively, we potentially have access to a relatively larger and more diverse offline dataset that covers a much richer subset of the state-action space. Still, any approach that augments the data of an agent in this manner must address the possibly large heterogeneity amongst the agents, which is challenging as we do not observe the characteristics that make agents heterogeneous. Inspired by the literature on collaborative filtering for recommendation systems, we posit that the transition dynamics across agents can be represented as a latent function of latent factors associated with agents, states, and actions. In doing so, we establish that this function is well-

approximated by a “low-rank” decomposition of separable agent, state, and action latent functions (Theorem 1). Hence, for any finite sampling of the state and action spaces, accurate model learning for each agent with offline data—generated from any policy—can be reduced to estimating a low-rank tensor corresponding to agents, states, and actions. As such, low-rank tensors can provide a useful algorithmic lens to enable model learning with offline data in RL and we hope this work leads to further research studying the relationship between these seemingly disparate fields.

Algorithmic — regularizing via a latent factor model. As a consequence of our low-rank representation result, we propose a natural neural network architecture that respects the constraints induced by the factorization across agents, states, and actions (Section 5). It is this principled structure, which accounts for agent heterogeneity and regularizes the model learning, that ensures the success of our approach despite access to only scarce and heterogeneous data.

Experimental — extensive benchmarking. Using standard environments from the OpenAI gym, we extensively benchmark PerSim against two state-of-the-art methods: a model-based online RL method (Lee et al., 2020) and a model-free offline RL method (Fujimoto et al., 2019). See Section 2 for our rationale in choosing these benchmarks. Below, we highlight four conclusions we reach from our experiments: (i) Despite access to only a single trajectory from each agent (and no access to the covariates that drive agent heterogeneity), PerSim produces accurate personalized simulators for each agent; (ii) Both benchmarking algorithms perform poorly for the data availability we consider, even on simple baseline environments such as MountainCar and Cartpole, which are traditionally considered to be “solved”. (iii) PerSim is able to robustly extrapolate outside the policy used to generate the offline dataset, even if the policy is highly sub-optimal (e.g., actions are sampled uniformly at random). (iv) As corroboration of our latent factor representation, we find that across all environments, the learned agent-specific latent factors correspond very closely with the latent source of heterogeneity amongst agents; we re-emphasize this is despite PerSim not getting access to the agent covariates. To visualize the above discussion, see Figure 1 for a depiction of the learned latent

agent factors and Figure 2 for the relative prediction accuracy of the learned model using PerSim versus (Lee et al., 2020).

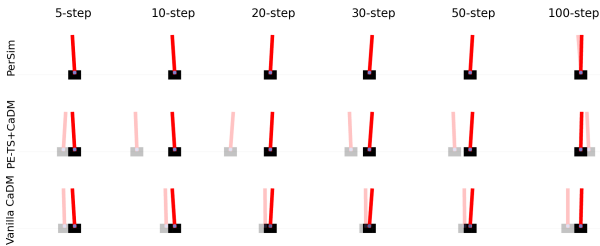


Figure 2. Visualization of the prediction accuracy of the various learned models for CartPole. Actual and predicted states are denoted by the opaque and translucent objects, respectively.

2. Related Work

Due to space constraints, we present a short overview of the related RL literature below. A more detailed description of related works can be found in Appendix B.

There are two sub-fields within RL that are of particular relevance: (i) model-based online RL and (ii) model-free offline RL. (i) In the model-based RL literature, the transition dynamics (simulator) is learnt and subsequently utilized for policy learning. These methods have been found to have far better data efficiency compared to their model-free counterparts (Wang et al., 2019; Chua et al., 2018; Clavera et al., 2018; Kurutach et al., 2018; Kaiser et al., 2019; Hafner et al., 2019). However, the current model-based literature mostly focuses on the setting where one can adaptively sample trajectories in an online manner during model-learning. A few recent works (Lee et al., 2020; Nagabandi et al., 2018a) have considered agent heterogeneity. We compare with (Lee et al., 2020) given its strong performance in handling heterogeneous agents. (ii) In the model-free offline RL literature, one uses a pre-recorded dataset to directly learn a policy, i.e., without first learning a model. Thus far, the vast majority of offline RL methods are model-free and designed for settings that allow access to numerous trajectories from a single agent, i.e., no agent heterogeneity (Fujimoto et al., 2019; Kumar et al., 2019; Larocche et al., 2019; Liu et al., 2020; Wu et al., 2019; Agarwal et al., 2020c; Kumar et al., 2020). To study how much offline methods suffer if agent heterogeneity is introduced, we compare with (Fujimoto et al., 2019) given its strong performance with offline data. We choose these two comparisons as they come from well-established literatures but their abilities to simultaneously handle agent heterogeneity and sparse offline data has yet to be studied.

Model-based offline RL is still a relatively nascent field. Two recent excellent works (Kidambi et al., 2020; Yu et al., 2020) have shown that, in certain settings, model-based offline methods can outperform their model-free counterparts on benchmark environments. (Yu et al., 2020) shows this is possible using existing online model-based methods with minimal changes to the algorithms. However, both works restrict attention to the setting where there is just one agent

of interest and a large number of observations from that agent are available. Extending these model-based offline RL methods to work with sparse data from heterogeneous agents, possibly by building upon the latent low-rank functional representation we propose, remains interesting future work.

3. Problem Statement

We consider the standard RL framework with N heterogeneous agents. Unless specified otherwise, we index agents with $n \in [N]$.¹ Formally, we describe our problem as a Markov Decision Process (MDP) that is defined as a tuple $(\mathcal{S}, \mathcal{A}, P_n, R_n, \gamma_n, \mu_n)$. Here, \mathcal{S} and \mathcal{A} denote the state and action spaces, respectively, which are common across agents. For every agent n , $P_n(s'|s, a)$ is the unknown transition kernel, $R_n(s, a)$ is the immediate reward received, $\gamma_n \in (0, 1)$ is the discounting factor, and μ_n is the initial state distribution.

Observations. We consider an offline RL setting where we observe a single trajectory of length T for each of the N heterogeneous agents. Formally, for each agent n and time step t , let $s_n(t) \in \mathcal{S}$, $a_n(t) \in \mathcal{A}$, and $r_n(t) \in \mathbb{R}$ denote the observed state, action, and reward. We denote our observations as $\mathcal{D} = \{(s_n(t), a_n(t), r_n(t)) : n \in [N], t \in [T]\}$.

Goals. We state our two primary goals below.

“Personalized” trajectory prediction. For a given agent n and state-action pair $(s, a) \in \mathcal{S} \times \mathcal{A}$, we would like to estimate $\mathbb{E}[s'_n | (s_n, a_n) = (s, a)]$, i.e., given the observations \mathcal{D} , we would like to build a “personalized” simulator (i.e., a model of the transition dynamic) for each agent n .

“Personalized” model-based policy learning. To test the efficacy of the personalized simulator, we would like to subsequently use it to learn a good decision-making policy for agent n , denoted as $\pi_n : \mathcal{S} \rightarrow \mathcal{A}$, which takes as input a given state and produces a corresponding action.

4. Latent Low-Rank Factor Representation

To address the goals of this work, we introduce a latent factor model for the transition dynamics. Leveraging latent factors have been successful in recommendation systems for overcoming heterogeneity of users. Such models have also been shown to provide a “universal” representation for multi-dimensional exchangeable arrays, cf. (Aldous, 1981; Hoover, 1979). Indeed, our latent model holds for known environments such as MountainCar.

Assume $\mathcal{S} \subseteq \mathbb{R}^D$, i.e., the state is D -dimensional. Let s_{nd} refer to the d -th coordinate of s_n . We posit the transition dynamics (in expectation) obey the following model: for every agent n and state-action pair (s, a) ,

$$\mathbb{E}[s'_{nd} | (s_n, a_n) = (s, a)] = f_d(\theta_n, \rho_s, \omega_a), \quad (1)$$

where s'_{nd} denotes the d -th state coordinate after taking action a . Here, $\theta_n \in \mathbb{R}^{d_1}$, $\rho_s \in \mathbb{R}^{d_2}$, $\omega_a \in \mathbb{R}^{d_3}$ for some $d_1, d_2, d_3 \geq 1$ are latent feature vectors capturing

¹For any positive integer N , let $[N] = \{1, \dots, N\}$.

relevant information specific to the agent, state, and action; $f_d: \mathbb{R}^{d_1} \times \mathbb{R}^{d_2} \times \mathbb{R}^{d_3} \rightarrow \mathbb{R}$ is a latent function capturing the model relationship between these latent feature vectors. We assume f_d is L -Lipschitz and the latent features are bounded.

Assumption 1. Suppose $\theta_n \in [0, 1]^{d_1}$, $\rho_s \in [0, 1]^{d_2}$, $\omega_a \in [0, 1]^{d_3}$, and f_d is L -Lipschitz with respect to its arguments, i.e., $|f_d(\theta_{n'}, \rho_{s'}, \omega_{a'}) - f_d(\theta_n, \rho_s, \omega_a)| \leq L(\|\theta_{n'} - \theta_n\|_2 + \|\rho_{s'} - \rho_s\|_2 + \|\omega_{a'} - \omega_a\|_2)$.

For notational convenience, let $\tilde{f}_d: [N] \times \mathcal{S} \times \mathcal{A} \rightarrow \mathbb{R}$ be such that $\tilde{f}_d(n, s, a) = \mathbb{E}[s'_{nd} | (s_n, a_n) = (s, a)]$.

Theorem 1. Suppose Assumption 1 holds and without loss of generality, let $d_1, d_3 \leq d_2$. Then for all $d \in [D]$ and any $\delta > 0$, there exists $h_d: [N] \times \mathcal{S} \times \mathcal{A} \rightarrow \mathbb{R}$, such that $h_d(n, s, a) = \sum_{\ell=1}^r u_\ell(n) v_\ell(s, d) w_\ell(a)$ with $r \leq C\delta^{-(d_1+d_3)}$ and $\|h_d - \tilde{f}_d\|_\infty \leq 2L\delta$, where C is an absolute constant.

Theorem 1 suggests that under the model in (1), the transition dynamics are well approximated by a low-rank order-three functional tensor representation. In fact, as we show below, for a classical non-linear dynamical system, it is exact.

An example. We show the MountainCar transition dynamics (Brockman et al., 2016) exactly satisfies this low-rank tensor representation. In MountainCar, the state $s_n = [s_{n1}, s_{n2}]$ consists of car (agent) n 's position and velocity, i.e., $\mathcal{S} \subseteq \mathbb{R}^2$; the action a_n is a scalar that represents the applied acceleration, i.e., $\mathcal{A} \subseteq \mathbb{R}$. For car n , parameterized by gravity g_n , the (deterministic) transition dynamics given action a_n are

$$\begin{aligned} s'_{n1} &= s_{n1} + s_{n2} - \frac{g_n \cos(3s_{n1})}{2} + \frac{a_n}{2}, \\ s'_{n2} &= s_{n2} - g_n \cos(3s_{n1}) + a_n. \end{aligned}$$

Proposition 1. In MountainCar, $r = 3$.

Model Learning & Tensor Estimation. Consider any finite sampling of the states $\tilde{\mathcal{S}} \subset \mathcal{S}$ and actions $\tilde{\mathcal{A}} \subset \mathcal{A}$. Let $\mathcal{X} = [X_{nsad}] \in \mathbb{R}^{N \times |\tilde{\mathcal{S}}| \times |\tilde{\mathcal{A}}| \times D}$ be the order-four tensor, where $X_{nsad} = f_d(\theta_n, \rho_s, \omega_a)$. Hence, to learn the model of transition dynamics for all the agents over $\tilde{\mathcal{S}}, \tilde{\mathcal{A}}$, it is sufficient to estimate the tensor, \mathcal{X} , from observed data. The offline data collected for a given policy induces a corresponding observation pattern of this tensor. Whether the complete tensor is recoverable, is determined by this induced sparsity pattern and the rank of \mathcal{X} . Notably, Theorem 1 suggests that \mathcal{X} is low-rank under mild regularity conditions. Therefore, the question of model identification, i.e., completing the tensor \mathcal{X} , boils down to conditions on the offline data in terms of the observation pattern that it induces in the tensor. In the existing tensor estimation literature, there are few sparsity patterns for which the underlying tensor can be provably recovered, provided \mathcal{X} has a low-rank structure. They include: (i) each entry of the tensor is observed independently at random with sufficiently high-probability (Barak & Moitra, 2016; Montanari & Sun, 2018; Shah & Yu, 2019); (ii) the entries that are observed are *block-structured* (Agarwal et al., 2020b; Shah et al., 2020). However, the most general set of conditions on the sparsity pattern under which the underlying tensor can be

faithfully estimated, i.e., the model is identified for our setup, remains an important and active area of research. In addition, when the state and action spaces are not finite (e.g., MountainCar), we are interested in estimating a low-rank tensor function, which is generally not considered in the literature.

5. PerSim Algorithm

We now detail our proposed algorithm which is composed of two steps: (i) build a personalized simulator for each agent n given offline observations \mathcal{D} , which is comprised of a single trajectory per agent; (ii) learn a personalized decision-making policy using MPC.

Step 1. Learning Personalized Simulators. Theorem 1 suggests that the transition dynamics can be represented as a low-rank tensor function with latent functions associated with the agents, states, and actions. This guides the design of a simple, regularized neural network architecture: we use three separate neural networks to learn the agent, state, and action latent functions, i.e., we remove any edges between these three neural networks. See Figure 1 for a visual depiction of our proposed architecture. Specifically, to estimate the next state for a given agent n and state-action pair $(s, a) \in \mathcal{S} \times \mathcal{A}$, we learn the following functions:

1. An agent encoder $g_u: [N] \rightarrow \mathbb{R}^r$, parameterized by ψ , which estimates the latent function associated with an agent, i.e., $\hat{u}(n) = g_u(n; \psi)$.
2. A state encoder $g_v: \mathcal{S} \rightarrow \mathbb{R}^{D \times r}$ parameterized by ϕ , which estimates D latent functions, where each vector is associated with the corresponding state coordinate, i.e., $\hat{v}(s) := (\hat{v}(s, 1), \dots, \hat{v}(s, D))^T = g_v(s; \phi)$.
3. An action encoder $g_w: \mathcal{A} \rightarrow \mathbb{R}^r$ parameterized by θ , which estimates the latent function associated with the action, i.e., $\hat{w}(a) = g_w(a; \theta)$.

Then, our estimate of the expected the d -th coordinate of the next state is given by

$$\hat{\mathbb{E}}[s'_{nd} | (s_n, a_n) = (s, a)] = \sum_{\ell=1}^r \hat{u}_\ell(n) \hat{v}_\ell(s, d) \hat{w}_\ell(a).$$

We optimize our agent, state, and action encoders by minimizing the squared loss:

$$\mathcal{L}(s, a, n, s'; \psi, \phi, \theta) = \sum_{d=1}^D \left(s'_{nd} - \sum_{\ell=1}^r \hat{u}_\ell(n) \hat{v}_\ell(s, d) \hat{w}_\ell(a) \right)^2.$$

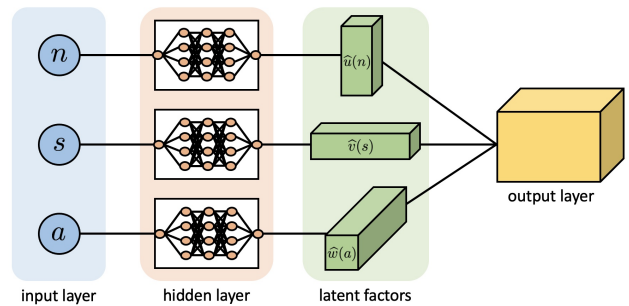


Figure 3. Neural Network Architecture

Step 2. Learning a Decision-making Policy. We use MPC to select the next action, as is done in (Lee et al., 2020). Specifically, we sample C candidate action sequences of length h , which we denote as $\{a_1^{(i)}, \dots, a_h^{(i)}\}_{i=1}^C$. The actions are sampled using the cross entropy method in environments with continuous action spaces and the random shooting method in environments with discrete action space (Camacho & Alba, 2013; Botev et al., 2013).

Since the offline data may not span the entire state-action space, planning using a learned simulator without any regularization may result in “model exploitation” (Levine et al., 2020). To overcome this issue, we gauge the model uncertainty, as is common in the literature, as follows. We train an ensemble of M simulators $\{g_u^{(m)}, g_s^{(m)}, g_a^{(m)}\}_{m=1}^M$. Then, for $i \in [C]$, $m \in [M]$, we evaluate the discounted reward of performing the i -th action sequence as estimated by the m -th simulator, which we denote by $r_m^{(i)}$. Specifically,

$$r_m^{(i)} = \sum_{t=1}^h \gamma^t R(\hat{s}_t^{(m,i)}, a_t^{(i)}),$$

where $\hat{s}_t^{(m,i)}$ is the predicted trajectory according to the m -th simulator and the sequence of actions $\{a_1^{(i)}, \dots, a_h^{(i)}\}$, γ is the discounting factor, and R is the reward function (which we assume is known, as is done in prior works (Lee et al., 2020; Kidambi et al., 2020)). Finally, we choose the first element from the sequence of actions with the best *minimum* reward across the M simulators, i.e., the sequence $\{a_1^{(i^*)}, \dots, a_h^{(i^*)}\}$, where $i^* = \operatorname{argmax}_{i \in [C]} \min_{m \in [M]} r_m^{(i)}$.

In our experiments, we find that the simple technique of using the state difference instead of the raw state improves performance. For a detailed description of the algorithm, including the pseudo-code, please refer to Appendix D.

6. Experiments

In this section, through a systematic collection of experiments on a variety of benchmark environments, we demonstrate that PerSim consistently outperforms state-of-the-art model-based and offline model-free RL algorithms, in terms of prediction error and reward, for the data regime we consider.

6.1. Setup and Benchmarks

We evaluate PerSim on benchmark environments from the OpenAI Gym (Brockman et al., 2016). A detailed description of each environment can be found in Appendix E. Due to space constraints, we focus on MountainCar, CartPole, and HalfCheetah in this section. However, the results in these environments are indicative of the overall conclusions.

Heterogeneous Agents. We introduce agent heterogeneity across the various environments by modifying the covariates that characterize the transition dynamics of an agent. This is in line with what has been done in the literature (Lee et al., 2020) to study algorithmic robustness to agent heterogeneity. The range of parameters we consider for each of the three

environments is given in Table 1; for example, we create heterogeneous agents in MountainCar by varying the gravity parameter of a car (agent) within the interval $[0.0001, 0.0035]$. See Appendix E for a detailed description of how we vary agent covariates in each environment.

For each environment, we uniformly sample 500 covariates (i.e., heterogeneous agents) from the parameter ranges displayed in Table 1. We then select five of the 500 agents to be our “test” agents, i.e., these are the agents for which we report the prediction error and eventual reward for the various RL algorithms. Our rationale for selecting these five agents is as follows: one of the five is the default covariate parameter in an environment; the other four are selected so as to cover the “extremes” of the parameter range. Due to space constraints, we show results for three test agents in this section; the results for the remaining two agents can be found in Appendix F. We note that the conclusions we draw from our experiments continue to hold over all test agents we evaluate on.

Offline Data from Sub-optimal Policies. To study how robust the various RL algorithms are to the “optimality” of the sampling policy used to generate the historical trajectories, we create four offline datasets of 500 trajectories (one per agent) for each environment as follows:

(i) *Pure policy.* For each agent, actions are sampled according to a fixed policy that has been trained to achieve “good” performance. Specifically, for each environment, we first train a policy in an online fashion for the five agents shown in Table 1. We pick the training agents to be uniformly spread throughout the training range to ensure reasonable performance for all agents. See Appendix E for details about the average reward achieved across all agents using this procedure. For MountainCar and CartPole, we use DQN (Mnih et al., 2015) to train the sampling policy; for HalfCheetah, we use TD3 (Fujimoto et al., 2018). The policies are trained to achieve rewards of approximately -200, 120, and 3000 for MountainCar, CartPole, and HalfCheetah, respectively. Then for each of the 500 agents, we sample one trajectory using the policy trained on the training agent with the closest parameter value.

(ii) *Random.* Actions are selected uniformly at random.

(iii/iv) *Pure- ϵ -20/Pure- ϵ -40.* For Pure- ϵ -20/40, actions are selected uniformly at random with probability 0.2/0.4, respectively, and selected via the pure policy otherwise.

The “pure policy” dataset has relatively optimal transition dynamics for each agent compared to the other three policies. This is likely the ideal scenario when we only have access to limited offline data. However, such an ideal sampling procedure is hardly met in practice. Real-world data often contains at least some amount of “trial and error” in terms of how actions are chosen; we model this by sampling a fraction of the trajectory at random.

Benchmarking Algorithms. We compare with two state-of-the-art RL algorithms, one from the online model-based literature and the other from the offline model-free literature.

Table 1. Environment parameters used for experiments.

Environment	Parameter range	Test agents	Policy training agents
MountainCar	gravity $\in [0.0001, 0.0035]$	{0.0001, 0.0005, 0.0010, 0.0025, 0.0035}	{0.0003, 0.00075, 0.00175, 0.0025, 0.0030}
CartPole	length $\in [0.15, 0.85]$ force $\in [2.0, 18]$	{(2.0,0.5), (10.0,0.5), (18.0, 0.5), (10.0,0.85), (10.0,0.15)}	{(6.0,0.5), (14.0,0.5), (10.0,0.5), (10.0,0.675), (10.0, 0.325)}
HalfCheetah	relative mass $\in [0.2, 1.8]$ relative damping $\in [0.2, 1.8]$	{(0.3,1.7), (1.7,0.3), (0.3, 0.3), (1.7,1.7), (1.0,1.0)}	{(0.6,1.4), (1.4,0.6), (0.6, 0.6), (1.4,1.4)}

In Appendix D, we give implementation details.

Vanilla CaDM + PE-TS CaDM (Lee et al., 2020). As aforementioned, we choose CaDM as a baseline given its superior performance against other popular model-based (and meta-learning) methods in handling heterogeneous agents. CaDM tackles heterogeneity by learning a context vector using the recent trajectory of a given agent, with a common context encoder across all agents. Since CaDM is a model-based method, we compare against two CaDM variants discussed in (Lee et al., 2020) with respect to both model prediction error and eventual reward.

BCQ-P + BCQ-A (Fujimoto et al., 2019). BCQ is an offline model-free RL method that has been shown to exhibit excellent performance in the standard offline setting, i.e., numerous trajectories collected of a single agent. In light of this, we consider two BCQ baselines: (i) BCQ-Population (or BCQ-P), where a *single* policy is trained using data from all available (heterogeneous) agents, i.e., all 500 observed trajectories; (ii) BCQ-Agent (or BCQ-A), where a separate policy is learned for each of the test agents using just the single observed trajectory associated with that test agent. We compare PerSim against both BCQ variants with respect to the eventual reward in order to study the effect that data scarcity and agent heterogeneity can have on standard offline RL methods.

6.2. Model Learning: Prediction Error

The core of PerSim is to build a personalized simulator for each agent. This is also the case for the two model-based methods we compare against, Vanilla CaDM and PE-TS CaDM. Thus, for each of these algorithms, we first evaluate the accuracy of the learned transition dynamics for each agent, focusing on long-horizon model prediction. Specifically, given an initial state and an unseen sequence of 50 actions, the task is to predict the next 50-step state trajectory for the test agents. The sequence of 50 actions are chosen according to an unseen test policy that is different than the policies used to sample the training dataset. Precisely, the test policies are fitted via DQN for MountainCar and CartPole and via TD3 for HalfCheetah for the agent with the default covariate parameters. The test policies were such that they achieved rewards of -150, 150, and 4000 for the MountainCar, CartPole and HalfCheetah environments, respectively.

For each environment and for each of the three model-based RL algorithms (PerSim, Vanilla CaDM, and PE-TS CaDM), we train four separate models using each of the four offline datasets described earlier. We repeat the process 200 times (totaling 200 trajectories for each test agent) and report the

Table 2. Prediction Error: MountainCar

Data	Method	0.0001	0.0025	0.0035
Pure	PerSim	0.025 (0.995)	0.015(0.984)	0.028 (0.939)
	Vanilla CaDM	0.709 (-3.326)	0.155 (-0.824)	0.142 (-1.391)
	PE-TS CaDM	0.789 (-4.203)	0.440 (-8.849)	0.438 (-11.44)
Random	PerSim	0.001 (1.000)	0.001 (1.000)	0.001 (1.000)
	Vanilla CaDM	0.731 (-4.673)	0.165 (-0.581)	0.143 (-0.940)
	PE-TS CaDM	0.792 (-4.380)	0.323 (-4.253)	0.316 (-4.845)
Pure- ϵ -20	PerSim	0.008 (0.998)	0.003 (0.999)	0.004 (0.998)
	Vanilla CaDM	0.696 (-3.420)	0.160 (-0.721)	0.144 (-1.295)
	PE-TS CaDM	0.791 (-4.294)	0.357 (-5.846)	0.353 (-6.691)
	Vanilla CaDM	0.619 (-3.558)	0.155 (-0.619)	0.144 (-1.174)
	PE-TS CaDM	0.780 (-4.312)	0.366 (-6.443)	0.363 (-7.580)

mean root-mean-squared error (RMSE) over all 50-steps and over all 200 trajectories. In addition to RMSE, we provide the median R^2 (in parentheses within the tables) to facilitate a better comparison in terms of relative error. The results are summarized in Tables 2, 3, and 4 for MountainCar, CartPole, and HalfCheetah, respectively. Further experimental results regarding prediction error can be found in Appendix F.

Table 3. Prediction Error: CartPole

Data	Method	(2/0.5)	(10/0.85)	(10/0.15)
Pure	PerSim	0.003 (1.000)	0.003 (1.000)	0.080 (0.994)
	Vanilla CaDM	3.190 (-0.698)	6.712 (-1.682)	12.31 (-1.953)
	PE-TS CaDM	2.940 (-7.009)	5.933 (-1.738)	12.24 (-2.207)
Random	PerSim	0.070 (0.683)	0.136 (0.964)	1.143 (-0.607)
	Vanilla CaDM	3.414 (-1.847)	4.351 (-1.997)	10.76 (-2.126)
	PE-TS CaDM	1.976 (-12.44)	2.043 (-2.620)	10.32 (-2.183)
Pure- ϵ -20	PerSim	0.004 (1.000)	0.004 (1.000)	0.170 (0.993)
	Vanilla CaDM	1.443 (-3.972)	2.614 (-0.789)	8.860 (-1.027)
	PE-TS CaDM	2.738 (-7.436)	5.618 (-1.780)	12.11 (-2.200)
Pure- ϵ -40	PerSim	0.008 (0.999)	0.015 (0.998)	0.232 (0.922)
	Vanilla CaDM	1.792 (-21.912)	0.924 (-6.017)	8.848 (-2.685)
	PE-TS CaDM	2.795 (-6.400)	5.659 (-1.925)	12.28 (-2.418)

PerSim Accurately Learns Personalized Simulators.

Across environments and test agents, PerSim consistently outperforms Vanilla CaDM and PE-TS CaDM by significant margins. RMSE for PerSim is notably lower by orders of magnitude. Indeed, R^2 for PerSim is generally high, while the two CaDM variants yield uniformly negative R^2 across experiments, indicating that they are worse than simply predicting the average state across the test trajectory. Notably, despite the challenging data availability, PerSim continues to deliver reasonably good predictions for each agent in HalfCheetah, which has a relatively high-dimensional state space (in particular, it is 18-dimensional). The only notable exception, though with good reason, is in CartPole under random data

Table 4. Prediction Error: HalfCheetah

Data	Method	(0.3/1.7)	(1.7/0.3)	(0.3/0.3)
Pure	PerSim	1.258 (0.924)	5.303 (0.339)	5.830 (0.701)
	Vanilla CaDM	114.0 (-2.354)	108.1 (-1.264)	119.4 (-0.535)
	PE-TS CaDM	128.7 (-12.03)	132.1 (-8.116)	130.3 (-5.035)
Random	PerSim	1.419 (0.921)	4.758 (0.451)	6.917 (0.759)
	Vanilla CaDM	75.15 (-1.424)	74.14 (-0.726)	80.62 (-0.339)
	PE-TS CaDM	83.68 (-8.292)	86.23 (-5.076)	86.35 (-3.070)
Pure- ϵ -20	PerSim	1.318 (0.930)	4.880 (0.432)	4.792 (0.782)
	Vanilla CaDM	74.69 (-1.884)	76.63 (-0.897)	80.89 (-0.457)
	PE-TS CaDM	93.20 (-9.709)	96.10 (-6.053)	95.67 (-3.560)
Pure- ϵ -40	PerSim	1.274 (0.929)	4.719 (0.457)	4.410 (0.779)
	Vanilla CaDM	78.89 (-1.907)	80.55 (-0.929)	82.72 (-0.458)
	PE-TS CaDM	89.44 (-9.083)	92.14 (-5.461)	91.78 (-3.205)

where extremely short trajectories are observed due to early termination when applying random actions.

Rethinking Model-based RL for Our Setting. Altogether, these results indicate that existing model-based RL methods cannot effectively learn a model of the transition dynamics simultaneously across heterogeneous agents if only given access to sparse offline data. It has been exhibited (Janner et al., 2019; Yu et al., 2020; Levine et al., 2020) that certain model-based methods that were originally targeted for the online setting can potentially still deliver reasonable performance with offline data and minimal algorithmic change. Our experiments offer evidence that model-based RL methods, even those which are optimized to work with heterogeneous agents, do not provide a “plug-in” solution for the particular data availability we consider. In contrast, our latent factor approach does seem to efficiently learn these dynamics given access to the exact same offline dataset. For a more visual representation of this phenomenon, refer back to Figure 2 in Section 1, which shows the predicted and actual state for different horizon lengths in CartPole; there, we see that our learned personalized simulator consistently produces state predictions that closely match the actual state observed from the true environment. Additional visualizations of the learned simulator across environments can be found in Appendix F.

Latent Factors Capture Agent Heterogeneity. The poor performance of standard model-based RL methods for the data availability setting we consider emphasizes the need for new principled approaches. Ours is one such approach, where we posit a low-rank latent factor representation of the agents, states, and actions. To further validate our approach, we visualize the learned latent agent factors associated with the 500 heterogeneous agents in each environment in Figure 1 of Section 1. Pleasingly, across environments, the latent factors correspond closely with the heterogeneity across agents.

6.3. Policy Performance: Average Reward

In this section, we evaluate the average reward achieved by PerSim compared to several state-of-the-art model-based and model-free offline RL methods. For the model-based methods, we follow (Lee et al., 2020) in utilizing MPC to make policy decisions on top of the learned model. We include an

additional baseline, “True env + MPC”, where we apply MPC on top of the actual ground-truth environment; this allows us to quantify the difference in reward when using MPC with the actual environment versus the learned simulators. For the two model-free BCQ methods, BCQ-P and BCQ-A, we can directly apply the policy resulted from the learned Q-value.

We evaluate the performance of each method using the average reward over 20 episodes for the model-based methods and the average reward over 100 episodes for the model-free methods. We repeat each experiment five times and report the mean and standard deviation. In Tables 5, 6, and 7, we present the results for MountainCar, CartPole, and HalfCheetah, respectively. Further experimental results regarding reward can be found in Appendix F.

Table 5. Reward: MountainCar.

Data	Method	0.0001	0.0025	0.0035
Pure	PerSim	-53.35±2.55	-191.81±4.44	-213.1±3.59
	Vanilla CaDM	-87.60±3.75	-500.0±0.00	-500.0±0.00
	PE-TS CaDM	-79.27±2.72	-500.0±0.00	-500.0±0.00
	BCQ-P	-67.60±22.3	-267.8±202.	-295.1±180.
	BCQ-A	-44.79±0.08	-380.7±170.	-500.0±0.00
Random	PerSim	-53.66±0.75	-198.8±6.77	-198.7±24.2
	Vanilla CaDM	-85.73±11.8	-500.0±0.00	-500.0±0.00
	PE-TS CaDM	-156.6±3.05	-500.0±0.00	-500.0±0.00
	BCQ-P	-500.0±0.00	-500.0±0.00	-500.0±0.00
	BCQ-A	-500.0±0.00	-500.0±0.00	-500.0±0.00
Pure- ϵ -20	PerSim	-48.75±3.64	-198.1±7.11	-202.2±23.45
	Vanilla CaDM	-81.53±3.74	-500.0±0.00	-500.0±0.00
	PE-TS CaDM	-86.80±4.11	-500.0±0.00	-500.0±0.00
	BCQ-P	-71.21±24.4	-286.6±196.	-328.3±158.
	BCQ-A	-364.5±180.	-260.6±51.4	-204.5±68.9
Pure- ϵ -40	PerSim	-48.60±2.83	-198.7±4.58	-202.7±21.0
	Vanilla CaDM	-80.70±2.52	-500.0±0.00	-500.0±0.00
	PE-TS CaDM	-86.23±4.11	-500.0±0.00	-500.0±0.00
	BCQ-P	-50.01±7.50	-373.6±180.	-352.0±211.
	BCQ-A	-94.87±0.88	-358.7±201.	-486.5±20.6
	True env+MPC	-53.95±4.10	-182.9±22.9	-197.5±20.7

As a high-level summary, PerSim consistently achieves higher rewards in almost all experiments and normally with very large margins. This not only reaffirms our prediction results in Section 6.2, but also is particularly encouraging for PerSim since the policy utilized is simply MPC and not optimized as done in model-free approaches. Furthermore, these results corroborate the appropriateness of our low-rank latent factor representation and our overall methodological framework as a principled solution to this challenging yet meaningful setting within offline RL. In what follows, we highlight and discuss additional interesting conclusions from these sets of experiments.

“Solved” Environments are Not Actually Solved. MountainCar and CartPole are commonly perceived as simple, “solved” environments within the RL literature. Yet, Tables 5 and 6 demonstrate that the offline setting with scarce and heterogeneous data impose unique challenges, and undoubtedly warrants a new methodology. We find state-of-the-art model-based and model-free methods perform poorly on

Table 6. Reward: CartPole.

Data	Method	(2/0.5)	(10/0.85)	(10/0.15)
Pure	PerSim	194.2 ± 3.23	186.3 ± 3.97	195.3 ± 2.10
	Vanilla CaDM	37.83± 2.37	23.74± 4.53	7.900± 1.31
	PE-TS CaDM	34.17± 1.14	22.64± 2.06	8.700± 0.58
	BCQ-P	166.2± 39.3	181.2± 13.5	182.8± 15.0
	BCQ-A	65.40± 67.5	79.20± 69.5	132.1± 85.0
Random	PerSim	178.4 ± 6.68	175.9 ± 7.34	119.1 ± 21.0
	Vanilla CaDM	35.10± 1.64	24.67± 4.70	8.550± 0.81
	PE-TS CaDM	33.03± 1.09	23.49± 2.60	9.920± 1.22
	BCQ-P	44.80± 34.0	57.91± 53.0	36.40± 36.0
	BCQ-A	43.90± 16.4	21.10± 5.81	39.50± 12.1
Pure- ϵ -20	PerSim	190.82 ± 1.63	184.4 ± 7.20	195.1 ± 3.20
	Vanilla CaDM	37.53± 2.07	22.10± 1.49	8.300± 0.79
	PE-TS CaDM	38.39± 4.23	24.81± 3.48	8.670± 0.37
	BCQ-P	98.90± 30.2	162.1± 15.5	86.10± 72.1
	BCQ-A	67.30± 62.2	65.60± 51.8	140.0± 80.6
Pure- ϵ -40	PerSim	183.7 ± 10.5	173.3 ± 5.50	195.9 ± 4.61
	Vanilla CaDM	36.46± 2.52	23.64± 1.54	8.390± 1.29
	PE-TS CaDM	40.47± 1.52	22.45± 2.20	8.800± 1.23
	BCQ-P	28.90± 6.80	31.80± 25.9	18.50± 11.1
	BCQ-A	34.60± 1.55	47.71± 48.7	23.20± 9.44
True env+MPC		198.9± 3.8	188± 23.0	199.1± 2.80

Table 7. Reward: HalfCheetah.

Data	Method	(0.3/1.7)	(1.7/0.3)	(0.3/0.3)
Pure	PerSim	378.5± 124	275.3± 118	612.4 ± 261
	Vanilla CaDM	-346.5± 162	-270.0± 25.7	-306.0± 87.6
	PE-TS CaDM	-405.8± 32.6	-251.8± 107	-380.5± 160
	BCQ-P	549.8 ± 322	2005.9 ± 152	-65.18± 92.8
	BCQ-A	-262.7± 96.6	-139.0± 236	165.6± 83.1
Random	PerSim	586.4 ± 121	352.7 ± 480	157.1 ± 463
	Vanilla CaDM	-271.8± 210	-135.5± 151	-223.2± 143
	PE-TS CaDM	-197.7± 27.6	-112.4± 31.4	-133.5± 22.4
	BCQ-P	-1.460± 0.16	-1.750± 0.22	-1.690± 0.19
	BCQ-A	279.6± 160	-44.05± 24.9	-75.03± 44.0
Pure- ϵ -20	PerSim	827.8 ± 353	617.7 ± 270	464.0 ± 377
	Vanilla CaDM	-120.1± 29.3	-96.10± 53.9	-138.4± 127
	PE-TS CaDM	-401.3± 10.5	-346.5± 58.7	-323.1± 86.7
	BCQ-P	254.6± 351	406.7± 71.1	385.9± 57.1
	BCQ-A	376.8± 102	84.66± 53.3	230.1± 10.0
Pure- ϵ -40	PerSim	477.7 ± 36.0	781.5 ± 130	769.8 ± 114
	Vanilla CaDM	-276.5± 50.5	-239.7± 70.7	-302.3± 44.1
	PE-TS CaDM	-198.9± 68.7	-180.0± 33.4	-194.6± 21.0
	BCQ-P	78.25± 199	173.8± 189	417.1± 155
	BCQ-A	269.2± 60.7	-181.5± 57.4	193.0± 31.8
True env+MPC		7459± 171	42893± 6959	66675± 9364

MountainCar and CartPole. In comparison, PerSim’s performance in these environments is close to that of MPC planning using the ground-truth environment, thereby confirming the success of learning the personalized simulators in Step 1 of our algorithm. Therefore, in certain rare cases (e.g., MountainCar test agent 0.0001) where BCQ has a comparable performance to PerSim, it is likely due to the limitations of MPC for policy planning. Further, the significant gain in reward of PerSim compared to the baseline methods continues to hold in HalfCheetah (see Table 7), which is considered a challenging high-dimensional environment.

PerSim Robustly Extrapolates with Sub-optimal Data. Crucially, across all environments and offline data gener-

ating processes, PerSim remains the most consistent and robust winner. This is a much desired property for offline RL. In real-world applications, the policy used to generate the offline dataset is likely unknown. Thus, for broad applicability of a RL methodological framework, it is vital that it is robust to sub-optimality in how the dataset was generated, e.g., the dataset may contain a significant amount of “trial and error” (i.e, randomized actions). Indeed, this is one of the primary motivations to use RL in such settings in the first place.

As mentioned earlier, the four offline datasets correspond to varying degrees of “optimality” of the policy used to sample agent trajectories. We highlight that PerSim achieves uniformly good reward, even with random data, i.e., the offline trajectories are produced using totally random actions. This showcases that by first learning a personalized simulator for each agent, PerSim is able to robustly *extrapolate* outside the policy used to generate the data, however sub-optimal that policy might be. In contrast, BCQ is not robust to such sub-optimality in the offline data generation. For example, for HalfCheetah, BCQ can achieve better results than PerSim only when trained on “optimal” offline data (i.e., pure policy). This is because BCQ, by design, is conservative and is regularized to only pick actions that are close to what is seen in the offline data. In summary, PerSim’s ability to successfully extrapolate, even when given sub-optimal offline data, makes it a suitable candidate for real-world applications.

7. Conclusion

In this work, we investigate RL in an offline setting, where we observe a single trajectory across heterogeneous agents under an unknown, potentially sub-optimal policy. This is particularly challenging for existing approaches even in “solved” environments such as MountainCar and CartPole. Our work, PerSim, offers a successful first attempt in simultaneously learning personalized policies across all agents under this data regime; we do so by first positing a principled low-rank latent factor representation, and then using it to build personalized simulators in a data-efficient manner. But there is much that remains unexplored. For example, in environments like HalfCheetah where the transition dynamics of each agent are harder to learn, the performance of PerSim is not comparable with the online setting, where one gets to arbitrarily sample trajectories for each agent. Of course, the considered data regime is fundamentally harder. Therefore, understanding the extent to which we can improve performance, using our low-rank latent factor approach or a different methodology altogether, remains to be established. Additionally, a rigorous finite-sample analysis for this setting, which studies the effect of the degree of agent heterogeneity, the diversity of the samples collected, etc. remains important future work. More generally, we believe that there are many fruitful inquiries under this challenging yet meaningful data regime for RL.

References

- Agarwal, A., Kakade, S., Krishnamurthy, A., and Sun, W. Flambe: Structural complexity and representation learning of low rank mdps. *arXiv preprint arXiv:2006.10814*, 2020a.
- Agarwal, A., Shah, D., and Shen, D. Synthetic interventions, 2020b.
- Agarwal, R., Schuurmans, D., and Norouzi, M. Striving for simplicity in off-policy deep reinforcement learning. 2019.
- Agarwal, R., Schuurmans, D., and Norouzi, M. An optimistic perspective on offline reinforcement learning. In *International Conference on Machine Learning*, pp. 104–114. PMLR, 2020c.
- Aldous, D. J. Representations for partially exchangeable arrays of random variables. *Journal of Multivariate Analysis*, 11(4):581–598, 1981.
- Barak, B. and Moitra, A. Noisy tensor completion via the sum-of-squares hierarchy. In *Conference on Learning Theory*, pp. 417–445. PMLR, 2016.
- Botev, Z. I., Kroese, D. P., Rubinstein, R. Y., and L’Ecuyer, P. The cross-entropy method for optimization. In *Handbook of statistics*, volume 31, pp. 35–59. Elsevier, 2013.
- Brockman, G., Cheung, V., Pettersson, L., Schneider, J., Schulman, J., Tang, J., and Zaremba, W. Openai gym. *arXiv preprint arXiv:1606.01540*, 2016.
- Camacho, E. F. and Alba, C. B. *Model predictive control*. Springer science & business media, 2013.
- Chua, K., Calandra, R., McAllister, R., and Levine, S. Deep reinforcement learning in a handful of trials using probabilistic dynamics models. *arXiv preprint arXiv:1805.12114*, 2018.
- Clavera, I., Rothfuss, J., Schulman, J., Fujita, Y., Asfour, T., and Abbeel, P. Model-based reinforcement learning via meta-policy optimization. In *Conference on Robot Learning*, pp. 617–629. PMLR, 2018.
- Deisenroth, M. and Rasmussen, C. E. Pilco: A model-based and data-efficient approach to policy search. In *Proceedings of the 28th International Conference on machine learning (ICML-11)*, pp. 465–472. Citeseer, 2011.
- Finn, C., Abbeel, P., and Levine, S. Model-agnostic meta-learning for fast adaptation of deep networks. In *International Conference on Machine Learning*, pp. 1126–1135. PMLR, 2017.
- Fujimoto, S., Hoof, H., and Meger, D. Addressing function approximation error in actor-critic methods. In *International Conference on Machine Learning*, pp. 1587–1596. PMLR, 2018.
- Fujimoto, S., Meger, D., and Precup, D. Off-policy deep reinforcement learning without exploration. In *International Conference on Machine Learning*, pp. 2052–2062. PMLR, 2019.
- Garcia, C. E., Prett, D. M., and Morari, M. Model predictive control: Theory and practice—a survey. *Automatica*, 25(3):335–348, 1989.
- Hafner, D., Lillicrap, T., Fischer, I., Villegas, R., Ha, D., Lee, H., and Davidson, J. Learning latent dynamics for planning from pixels. In *International Conference on Machine Learning*, pp. 2555–2565. PMLR, 2019.
- Hoover, D. N. Relations on probability spaces and arrays of random variables. *Preprint, Institute for Advanced Study, Princeton, NJ*, 2, 1979.
- Janner, M., Fu, J., Zhang, M., and Levine, S. When to trust your model: Model-based policy optimization. *arXiv preprint arXiv:1906.08253*, 2019.
- Jin, C., Yang, Z., Wang, Z., and Jordan, M. I. Provably efficient reinforcement learning with linear function approximation. In *Conference on Learning Theory*, pp. 2137–2143. PMLR, 2020.
- Kaiser, L., Babaeizadeh, M., Milos, P., Osinski, B., Campbell, R. H., Czechowski, K., Erhan, D., Finn, C., Kozakowski, P., Levine, S., et al. Model-based reinforcement learning for atari. *arXiv preprint arXiv:1903.00374*, 2019.
- Kalashnikov, D., Irpan, A., Pastor, P., Ibarz, J., Herzog, A., Jang, E., Quillen, D., Holly, E., Kalakrishnan, M., Vanhoucke, V., et al. Qt-opt: Scalable deep reinforcement learning for vision-based robotic manipulation. *arXiv preprint arXiv:1806.10293*, 2018.
- Kidambi, R., Rajeswaran, A., Netrapalli, P., and Joachims, T. Morel: Model-based offline reinforcement learning. *arXiv preprint arXiv:2005.05951*, 2020.
- Kumar, A., Fu, J., Soh, M., Tucker, G., and Levine, S. Stabilizing off-policy q-learning via bootstrapping error reduction. In *Advances in Neural Information Processing Systems*, pp. 11784–11794, 2019.
- Kumar, A., Zhou, A., Tucker, G., and Levine, S. Conservative q-learning for offline reinforcement learning. *arXiv preprint arXiv:2006.04779*, 2020.
- Kurutach, T., Clavera, I., Duan, Y., Tamar, A., and Abbeel, P. Model-ensemble trust-region policy optimization. *arXiv preprint arXiv:1802.10592*, 2018.
- Lange, S., Gabel, T., and Riedmiller, M. Batch reinforcement learning. In *Reinforcement learning*, pp. 45–73. Springer, 2012.

- Laroche, R., Trichelair, P., and Des Combes, R. T. Safe policy improvement with baseline bootstrapping. In *International Conference on Machine Learning*, pp. 3652–3661. PMLR, 2019.
- Lee, K., Seo, Y., Lee, S., Lee, H., and Shin, J. Context-aware dynamics model for generalization in model-based reinforcement learning. In *International Conference on Machine Learning*, pp. 5757–5766. PMLR, 2020.
- Levine, S., Finn, C., Darrell, T., and Abbeel, P. End-to-end training of deep visuomotor policies. *The Journal of Machine Learning Research*, 17(1):1334–1373, 2016.
- Levine, S., Kumar, A., Tucker, G., and Fu, J. Offline reinforcement learning: Tutorial, review, and perspectives on open problems. *arXiv preprint arXiv:2005.01643*, 2020.
- Liu, Y., Swaminathan, A., Agarwal, A., and Brunskill, E. Provably good batch reinforcement learning without great exploration. *arXiv preprint arXiv:2007.08202*, 2020.
- Luo, Y., Xu, H., Li, Y., Tian, Y., Darrell, T., and Ma, T. Algorithmic framework for model-based deep reinforcement learning with theoretical guarantees. *arXiv preprint arXiv:1807.03858*, 2018.
- Mnih, V., Kavukcuoglu, K., Silver, D., Rusu, A. A., Veness, J., Bellemare, M. G., Graves, A., Riedmiller, M., Fidjeland, A. K., Ostrovski, G., et al. Human-level control through deep reinforcement learning. *Nature*, 518(7540): 529, 2015.
- Montanari, A. and Sun, N. Spectral algorithms for tensor completion. *Communications on Pure and Applied Mathematics*, 71(11):2381–2425, 2018.
- Nagabandi, A., Clavera, I., Liu, S., Fearing, R. S., Abbeel, P., Levine, S., and Finn, C. Learning to adapt in dynamic, real-world environments through meta-reinforcement learning. *arXiv preprint arXiv:1803.11347*, 2018a.
- Nagabandi, A., Finn, C., and Levine, S. Deep online learning via meta-learning: Continual adaptation for model-based rl. *arXiv preprint arXiv:1812.07671*, 2018b.
- Sæmundsson, S., Hofmann, K., and Deisenroth, M. P. Meta reinforcement learning with latent variable gaussian processes. *arXiv preprint arXiv:1803.07551*, 2018.
- Schrittwieser, J., Antonoglou, I., Hubert, T., Simonyan, K., Sifre, L., Schmitt, S., Guez, A., Lockhart, E., Hassabis, D., Graepel, T., et al. Mastering atari, go, chess and shogi by planning with a learned model. *Nature*, 588(7839): 604–609, 2020.
- Shah, D. and Yu, C. L. Iterative collaborative filtering for sparse noisy tensor estimation. In *2019 IEEE International Symposium on Information Theory (ISIT)*, pp. 41–45. IEEE, 2019.
- Shah, D., Song, D., Xu, Z., and Yang, Y. Sample efficient reinforcement learning via low-rank matrix estimation. *arXiv preprint arXiv:2006.06135*, 2020.
- Silver, D., Hubert, T., Schrittwieser, J., Antonoglou, I., Lai, M., Guez, A., Lanctot, M., Sifre, L., Kumaran, D., Graepel, T., et al. Mastering chess and shogi by self-play with a general reinforcement learning algorithm. *arXiv preprint arXiv:1712.01815*, 2017a.
- Silver, D., Schrittwieser, J., Simonyan, K., Antonoglou, I., Huang, A., Guez, A., Hubert, T., Baker, L., Lai, M., Bolton, A., et al. Mastering the game of go without human knowledge. *Nature*, 550(7676):354–359, 2017b.
- Todorov, E., Erez, T., and Tassa, Y. Mujoco: A physics engine for model-based control. In *2012 IEEE/RSJ International Conference on Intelligent Robots and Systems*, pp. 5026–5033. IEEE, 2012.
- Van der Maaten, L. and Hinton, G. Visualizing data using t-sne. *Journal of machine learning research*, 9(11), 2008.
- Wang, T. and Ba, J. Exploring model-based planning with policy networks. *arXiv preprint arXiv:1906.08649*, 2019.
- Wang, T., Bao, X., Clavera, I., Hoang, J., Wen, Y., Langlois, E., Zhang, S., Zhang, G., Abbeel, P., and Ba, J. Benchmarking model-based reinforcement learning. *arXiv preprint arXiv:1907.02057*, 2019.
- Wu, Y., Tucker, G., and Nachum, O. Behavior regularized offline reinforcement learning. *arXiv preprint arXiv:1911.11361*, 2019.
- Yang, L. and Wang, M. Sample-optimal parametric q-learning using linearly additive features. In *International Conference on Machine Learning*, pp. 6995–7004. PMLR, 2019.
- Yu, T., Thomas, G., Yu, L., Ermon, S., Zou, J., Levine, S., Finn, C., and Ma, T. Mopo: Model-based offline policy optimization. *arXiv preprint arXiv:2005.13239*, 2020.

Supplementary Materials

A. Organization of Supplementary Materials

The supplementary materials consist of five main sections.

Related Work. In Appendix B, we give a detailed overview of the related literature.

Proofs for Section 4. In Appendix C, we give the proofs of Theorem 1 and Proposition 1.

Algorithm and Implementation Details. In Appendix D, we provide further details about the implementation and training procedure for PerSim and the RL methods we benchmark against.

Detailed Experimental Setup. In Appendix E, we detail the setup used to run our experiments. In Appendix E.1, we describe the OpenAI environments used. In Appendix E.2, we describe how we generate the offline training datasets for each environment.

Additional Experimental Results. In Appendix F, we give more detailed results for the experiments we run. In particular, we provide results for all five test agents in each environment (recall that, due to space constraints, we only show results for three of the five test agents in Section 6 of the main paper). In Appendix F.1, we provide comprehensive results for the long-horizon prediction accuracy of the model-based methods. In Appendix F.2, we provide comprehensive results for the achieved reward in the various environments for both the model-based and model-free methods. In Appendix F.3, we provide additional visualizations of the latent agent factors.

B. Related Work

Model-based Online RL. In model-based RL methods (Wang et al., 2019; Schrittwieser et al., 2020; Janner et al., 2019; Wang & Ba, 2019; Kaiser et al., 2019; Luo et al., 2018; Deisenroth & Rasmussen, 2011), the transition dynamics or simulator is learnt and subsequently utilized for policy learning. Compared to their model-free counterparts, model-based approaches, when successful, have proven to be far more data-efficient in terms of the number of samples required to learn a good policy and have shown to generalize better to unseen (state, action) tuples (Chua et al., 2018; Clavera et al., 2018; Kurutach et al., 2018; Kaiser et al., 2019; Hafner et al., 2019). Recently, such methods have also been shown to effectively deal with agent heterogeneity, e.g., (Lee et al., 2020) learns a context vector using the recent trajectory of a given agent, with a common context encoder across all agents. Several recent works also utilize the meta-learning framework (Finn et al., 2017) to quickly adapt the model for model-based RL (Sæmundsson et al., 2018; Nagabandi et al., 2018b;a). Thus far, the vast majority of the model-based RL literature has focused on the online setting, where transition dynamics are learned by adaptively sampling trajectories. Such online sampling helps these methods efficiently quantify and reduce uncertainty for unseen (state, action)-pairs. Further, there has been some work showing the success of online model-based RL approaches with offline data, with minimal change in the algorithm (Janner et al., 2019; Yu et al., 2020). This serves as additional motivation to compare with a state-of-the-art model-based RL method such as (Lee et al., 2020), which is designed to address agent heterogeneity.

Model-free Offline RL. As stated earlier, the offline RL paradigm (Lange et al., 2012; Levine et al., 2020) is meant to allow one to leverage large pre-recorded (static) datasets to learn policies. Such methods are particularly pertinent for situations in which interacting with the environment can be costly and/or unethical, e.g., healthcare, autonomous driving, social/economic systems. The vast majority of offline RL methods are model-free (Fujimoto et al., 2019; Kumar et al., 2019; Laroche et al., 2019; Liu et al., 2020; Wu et al., 2019; Agarwal et al., 2020c; Kumar et al., 2020). Despite their rapidly increasing popularity, traditional offline RL methods suffer from “distribution shift”, i.e., the policy learnt using such methods perform poorly on (state, action)-pairs that are unseen in the offline dataset (Kumar et al., 2019; Fujimoto et al., 2019; Agarwal et al., 2019; Levine et al., 2020). To overcome this challenge, offline RL methods design policies that are “close”, in an appropriate sense, to the observed behavioural policy in the offline dataset (Kumar et al., 2019; Wu et al., 2019; Fujimoto et al., 2019). They normally do so by directly regularizing the learnt policy (e.g. parameterized via the Q-function) based on the quantified level of uncertainty for a given (state, action)-pair. Most offline RL methods tend to be designed for the case where there is no agent heterogeneity. To study how much offline methods suffer if agent heterogeneity is introduced, we compare with one state-of-the-art offline RL method (Fujimoto et al., 2019).

Model-based Offline RL. Model-based offline RL is a relatively nascent field. Two recent excellent works (Kidambi et al., 2020; Yu et al., 2020) have shown that in certain settings, first building a model from offline data and then learning a policy outperforms state-of-the-art model-free offline RL methods on benchmark environments. By learning a model of the transition dynamics first, it allows such methods to trade-off the risk of leaving the behavioral distribution with the gains of exploring diverse states. However, the current inventory of model-based offline RL methods still require a large and diverse dataset for

each agent of interest—in fact, these methods restrict attention to the setting where there is just one agent of interest and one gets observations just from that one agent. Our approach effectively resolves the challenge via developing a principled and generic model representation. It is worth mentioning that albeit in different settings, several recent theoretical works have shown that structured MDPs (e.g., low-rank or linear transition model or value functions) can lead to provably efficient RL algorithms (Yang & Wang, 2019; Agarwal et al., 2020a; Jin et al., 2020; Shah et al., 2020). Extending the current model-based offline RL methods to work with sparse data from heterogeneous agents, possibly by building upon the latent low-rank tensor representation we propose, remains an interesting future work.

C. Theoretical Results

C.1. Proof of Theorem 1

Proof. We will construct the function h_d by partitioning the latent parameter spaces associated with agents, states, and actions. We will then complete the proof by showing that h_d is entry-wise close to \tilde{f}_d .

Partitioning the latent spaces to construct h_d . Fix some $\delta_1, \delta_3 > 0$. Since the latent row parameters θ_n come from a compact space $[0, 1]^{d_1}$, we can construct a finite covering or partitioning $P_1(\delta_1) \subset [0, 1]^{d_1}$ such that for any $\theta_n \in [0, 1]^{d_1}$, there exists a $\theta_{n'} \in P_1(\delta_1)$ satisfying $\|\theta_n - \theta_{n'}\|_2 \leq \delta_1$. By the same argument, we can construct a partitioning $P_3(\delta_3) \subset [0, 1]^{d_3}$ such that $\|\omega_a - \omega_{a'}\|_2 \leq \delta_3$ for any $\omega_a \in [0, 1]^{d_3}$ and some $\omega_{a'} \in P_3(\delta_3)$.

For each θ_n , let $p_1(\theta_n)$ denote the unique element in $P_1(\delta_1)$ that is closest to θ_n . Similarly, define $p_3(\omega_a)$ as the corresponding element in $P_3(\delta_3)$ that is closest to ω_a . We enumerate the elements of $P_1(\delta_1)$ as $\{\tilde{\theta}_1, \dots, \tilde{\theta}_{|P_1(\delta_1)|}\}$. Analogously, we enumerate the elements of $P_3(\delta_3)$ as $\{\tilde{\omega}_1, \dots, \tilde{\omega}_{|P_3(\delta_3)|}\}$. We now define h_d as follows:

$$h_d(n, s, a) = \sum_{i=1}^{|P_1(\delta_1)|} \sum_{j=1}^{|P_3(\delta_3)|} \mathbb{1}(p_1(\theta_n) = \tilde{\theta}_i) \mathbb{1}(p_3(\omega_a) = \tilde{\omega}_j) f_d(\tilde{\theta}_i, \rho_s, \tilde{\omega}_j).$$

\tilde{f}_d is well approximated by h_d . Here, we bound the maximum difference of any entry in \tilde{f}_d from h_d . Using the Lipschitz property of f_d (Assumption 1), we obtain for any (n, s, a) ,

$$\begin{aligned} & |\tilde{f}_d(n, s, a) - h_d(n, s, a)| \\ &= \left| f_d(\theta_n, \rho_s, \omega_a) - \sum_{i=1}^{|P_1(\delta_1)|} \sum_{j=1}^{|P_3(\delta_3)|} \mathbb{1}(p_1(\theta_n) = \tilde{\theta}_i) \mathbb{1}(p_3(\omega_a) = \tilde{\omega}_j) f_d(\tilde{\theta}_i, \rho_s, \tilde{\omega}_j) \right| \\ &= |f_d(\theta_n, \rho_s, \omega_a) - f_d(p_1(\theta_n), \rho_s, p_3(\omega_a))| \\ &\leq L(\|\theta_n - p_1(\theta_n)\|_2 + \|\omega_a - p_3(\omega_a)\|_2) \\ &\leq L(\delta_1 + \delta_3). \end{aligned}$$

This proves that \tilde{f}_d is entry-wise arbitrarily close to h_d .

Concluding the proof. It remains to write $h_d(n, s, a)$ as $\sum_{\ell=1}^r u_\ell(n) v_\ell(s, d) w_\ell(a)$ and bound the induced r . To that end, for $\ell = (i, j) \in [|P_1(\delta_1)|] \times [|P_3(\delta_3)|]$, we define

$$u_\ell(n) := \mathbb{1}(p_1(\theta_n) = \tilde{\theta}_i), \quad v_\ell(s, d) := f_d(\tilde{\theta}_i, \rho_s, \tilde{\omega}_j), \quad w_\ell(a) := \mathbb{1}(p_3(\omega_a) = \tilde{\omega}_j).$$

This allows us to write $r = |P_1(\delta_1)| \cdot |P_3(\delta_3)|$. Since each of the latent spaces is a unit cube of different dimensions, i.e., $[0, 1]^x$ with $x \in \{d_1, d_3\}$, we can simply create partitions $P_1(\delta_1), P_3(\delta_3)$ by creating grid of cubes of size δ_1 and δ_3 respectively. In doing so, the number of such cubes will scale as $|P_1(\delta_1)| \leq C\delta_1^{-d_1}, |P_3(\delta_3)| \leq C\delta_3^{-d_3}$, where C is an absolute constant. As such, $r \leq C\delta_1^{-d_1} \delta_3^{-d_3}$. Setting $\delta = \delta_1 = \delta_3$ completes the proof. \square

C.2. Proof of Proposition 1

Proof. To show that $r = 3$, it suffices to find $u(n), v(s_n, 1), v(s_n, 2), w(a_n) \in \mathbb{R}^3$ such that $h_d(n, s_n, a_n) = \sum_{\ell=1}^r u_\ell(n) v_\ell(s_n, d) w_\ell(a_n)$ for any $n \in [N]$, $s_n = [s_{n1}, s_{n2}] \in \mathcal{S}$, $a_n \in \mathcal{A}$, and $d \in \{1, 2\}$. In particular, we require that $u(n)$ can only depend on agent n , i.e., not on the action or state. Analogously, $v(s_n, 1)$ and $v(s_n, 2)$ can only depend on the state, and $w(a_n)$ can only depend on the action. Towards this, consider the following factors:

$$\begin{aligned} u(n) &= [1 \quad g_n \quad 1], & w(a_n) &= [1 \quad 1 \quad a_n], \\ v(s_n, 1) &= \left[s_{n1} + s_{n2} \quad -\frac{\cos(3s_{n1})}{2} \quad \frac{1}{2} \right], & v(s_n, 2) &= [s_{n2} \quad -\cos(3s_{n1}) \quad 1]. \end{aligned}$$

Recalling $h_1(n, s_n, a_n) = s_{n1} + s_{n2} - \frac{g_n \cos(3s_{n1})}{2} + \frac{a_n}{2}$ and $h_2(n, s_n, a_n) = s_{n2} - g_n \cos(3s_{n1}) + a_n$ completes the proof. \square

D. Algorithm and Implementation Details

D.1. Our Method

Step 1 Details: Learning Personalized Simulators. As explained in Section 5, the personalized simulators are effectively trained by learning g_u , g_v , and g_w , which correspond to the agent, state, and action encoders, respectively. Below, we detail the architecture used for each function.

1. **Agent encoder:** g_u . We use a single layer that takes in a one-hot encoder of the agent and returns an r -dimensional latent factor.
2. **State encoder:** g_v . We use a multilayer perceptron (MLP) with 1 hidden layer of 256 ReLU activated nodes for both MountainCar and CartPole, and an MLP with 3 hidden layers of (256,512,512) ReLU activated nodes for HalfCheetah.
3. **Action encoder:** g_w . In environments with discrete action spaces, i.e., MountainCar and CartPole, we use a single layer that takes in a one-hot encoder of the action and produce an r -dimensional latent factor. For HalfCheetah, we use an MLP with 2 hidden layers of (256,256) ReLU activated nodes.

We choose the tensor rank r to be 3, 5, and 20 for the MountainCar, CartPole, and HalfCheetah environments, respectively. The choice is made via cross validation from the set $\{3,5,10,15,20,30\}$. Specifically, 20% of the data points (selected randomly from different trajectories) are set aside for validation in the hyper-parameter selection process. Across all experiments, we train our simulators with a learning rate of 0.001, batch size of 256, and 300 epochs. Please refer to the pseudo-code in Algorithm 1 for a detailed description of the training procedure.

Algorithm 1 Training Personalized Dynamic Models

- 1: **Input:** Dataset \mathcal{D} , Rank r , Learning rate η , Batch size B , Number of epochs K
 - 2: **Output:** $g_u(\cdot; \psi)$, $g_v(\cdot; \phi)$, $g_w(\cdot; \theta)$
 - 3: Initialize ψ , ϕ , and θ
 - 4: **for** each epoch **do** :
 - 5: **for** each batch **do** :
 - 6: **for** $i = 1$ to B **do** :
 - 7: Sample $\{s_i, a_i, s'_i, n_i\} \sim \mathcal{D}$
 - 8: Compute $\Delta s_i \leftarrow s'_i - s_i$
 - 9: Get agent latent factor $\hat{u}(n_i) \leftarrow g_u(n_i; \psi)$
 - 10: Get state latent factor $\hat{v}(s_i) := [\hat{v}(s_i, d)]_{d \in [D]} \leftarrow g_v(s_i; \phi)$
 - 11: Get action latent factor $\hat{w}(a_i) \leftarrow g_w(a_i; \theta)$
 - 12: Get the error estimate $\mathcal{L}_i \leftarrow \|\Delta s_i - \sum_{\ell=1}^r \hat{u}_\ell(n_i) v_\ell(s_i) \hat{w}_\ell(a_i)\|_2^2$
 - 13: **end for**
 - 14: Update $\psi \leftarrow \psi - \eta \nabla_\psi \frac{1}{B} \sum_{i=1}^B \mathcal{L}_i$
 - 15: Update $\phi \leftarrow \phi - \eta \nabla_\phi \frac{1}{B} \sum_{i=1}^B \mathcal{L}_i$
 - 16: Update $\theta \leftarrow \theta - \eta \nabla_\theta \frac{1}{B} \sum_{i=1}^B \mathcal{L}_i$
 - 17: **end for**
 - 18: **end for**
-

Step 2 Details: Learning a Decision-making Policy. As outlined in Section 5, we use MPC to select the best action. For MountainCar and CartPole, we use random shooting to sample 1000 candidate actions with a planning horizon of 50 and 30, respectively. For HalfCheetah, we use the cross entropy method to sample 200 candidate actions with a planning horizon of 30. For all environments, we train $M = 5$ simulators and use a discounting factor $\gamma = 0.93$.

D.2. Benchmarking Algorithms

Vanilla CaDM + PE-TS CaDM. We use the implementation provided by the authors in (Lee et al., 2020).² To train on offline data, we modify the sampling procedure in the implementation. Specifically, we change it to sample from a replay buffer containing the recorded trajectories. Similar to our method, we use MPC with a planning horizon of 30 for CartPole and HalfCheetah, and 50 for MountainCar. We train the forward dynamic model, the backward dynamic model, and the context encoder for 100 iterations with a learning rate of 0.001. For PE-TS, as is done in (Lee et al., 2020), we use an ensemble of five dynamics models, and use twenty particles for trajectory sampling.

²<https://github.com/younggyoseo/CaDM>

BCQ-P +BCQ-A. We use the implementation provided by the authors in (Fujimoto et al., 2019).³ Specifically, we use discrete BCQ for MountainCar and CartPole, and continuous BCQ for HalfCheetah. For both BCQ-P and BCQ-A, we train the policy for 5.5×10^5 iterations.

E. Detailed Setup

E.1. Environments

In this paper, we carry out experiments on three environments from the OpenAI gym: two classical non-linear control environments, MountainCar and CartPole, and one Mujoco environment, HalfCheetah (Todorov et al., 2012). In what follows, we describe these three environments in detail.

MountainCar. In MountainCar, the goal is to drive a under-powered car to the top of a hill by taking the least number of steps.

- *Observation.* We observe $x(t), \dot{x}(t)$: the position and velocity of the car, respectively.
- *Actions.* There are three possible actions $\{0,1,2\}$: (0) accelerate to the left; (1) do nothing; (2) accelerate to the right.
- *Reward.* The reward is defined as

$$R(t) = \begin{cases} 1, & x(t) \geq 0.5 \\ -1, & \text{otherwise.} \end{cases}$$

- *Environment modification.* We vary the gravity within the range $[0.0001, 0.0035]$. Note that with a weaker gravity, the environment is trivially solved by directly moving to the right. On the other hand, with a stronger gravity, the car must drive left and right to build up enough momentum. See Table 1 for details about the parameter ranges and the test agents.

CartPole. In CartPole, a pole is attached to a cart moving on a frictionless track. The goal is to prevent the pole from falling over by moving the cart to the left or to the right, and to do so for as long as possible (maximum of 200 steps).

- *Observation.* We observe $x(t), \dot{x}(t), \theta(t), \dot{\theta}(t)$: the cart’s position, its velocity, the pole’s angle, and its angular velocity, respectively.
- *Actions.* There are two possible actions $\{0,1\}$: (0) push to the right; (1) push to the left.
- *Reward.* The reward is 1 for every step taken without termination. The environment terminates when the pole angle exceeds 12 degrees or when the cart position exceeds 2.4.
- *Environment modification.* As is done in (Lee et al., 2020), we vary the length of the pole and push force within the ranges $[0.15, 0.85]$ and $[2.0, 18.0]$, respectively. See Table 1 for details about the parameter ranges and the test agents.

HalfCheetah. In HalfCheetah, the goal is to move the cheetah as fast as possible. The cheetah’s body consists of 7 links connected via 6 joints.

- *Observation.* We observe an 18-dimensional vector that includes the angle and angular velocity of all six joints, as well as the 3-D position and orientation of the torso. Additionally, as is done in previous studies (Lee et al., 2020; Kidambi et al., 2020), we append the center of mass velocity to our state vector to enable computing the reward from observations.
- *Actions.* The action $a(t) \in [-1, 1]^6$ represents the torque applied at the six joints.
- *Reward.* The reward is defined as

$$R(t) = v(t) - 0.05 \|a(t)\|^2,$$

where $v(t)$ is the center of mass velocity at time t .

- *Environment modification.* As is done in (Lee et al., 2020), we scale the mass of every link and the damping of every joint by factors m and d , respectively. Specifically, we vary both m and d within the range $[0.2, 1.8]$. See Table 1 for details about the parameter ranges and the test agents.

E.2. Offline Datasets

As stated in Section 6, we generate four offline datasets for each environment with varying “optimality” of the sampling policy. Specifically, we generate 500 trajectories (one per agent) for each environment as per the following sampling procedures:

(i) Pure. In the Pure procedure, actions are sampled according to a fixed policy (for each agent) that has been trained to achieve “good” performance. That is, for each environment, we first train a policy using online model-free algorithms for the training agents shown in Table 1. Specifically, we train these logging policies using DQN (Mnih et al., 2015) for MountainCar and CartPole, and using TD3 for and HalfCheetah. We train these policies to achieve rewards of approximately -200, 120,

³<https://github.com/sfujim/BCQ>

3000, for MountainCar, CartPole, and HalfCheetah respectively. Then, to sample a trajectory for each of the 500 agents, we use the policy trained on the training agent with the closest parameter value.

(ii) **Random.** Actions are selected uniformly at random.

(iii) **Pure- ϵ -20.** Actions are selected uniformly at random with probability of 0.2, and selected via the pure policy otherwise.

(iv) **Pure- ϵ -40.** Actions are selected uniformly at random with probability of 0.4, and selected via the pure policy otherwise.

See Table 8 for details about the reward observed for the five test agents using these four sampling procedures, and the average reward and trajectory length achieved across all 500 agents.

Table 8. Observed reward and trajectory length in the four sampled datasets in each environment. Agent 1 to Agent 5 refer to the five test agents. The average is taken across all 500 agents.

Environment	Data	Observed Reward					Average	
		Agent 1	Agent 2	Agent 3	Agent 4	Agent 5	Average	Trajectory Length
MountainCar	Pure	-48.0	-50.0	-57.0	-171.0	-134.0	-112.926	113.914
	Random	-500.0	-500.0	-500.0	-500.0	-500.0	-496.324	496.344
	Pure-eps-2	-46.0	-54.0	-73.0	-165.0	-140.0	-155.252	156.214
	Pure-eps-4	-55.0	-64.0	-500.0	-264.0	-208.0	-227.278	228.18
CartPole	Pure	184	200	196	177	200	187.12	187.12
	Random	54	12	25	22	11	23.67	23.67
	Pure-eps-2	190	200	196	200	41	155.202	155.202
	Pure-eps-4	24.0	92.0	181.0	19.0	9.0	94.64	94.64
HalfCheetah	Pure	522.40	1246.32	251.25	2646.85	1011.99	1894.10	1000.00
	Random	-395.58	-65.77	-106.80	-150.01	-323.86	-251.75	1000.00
	Pure-eps-2	399.95	938.58	189.17	1742.85	1137.45	1121.52	1000.00
	Pure-eps-4	508.11	-115.94	128.64	1155.23	216.69	771.71	1000.00

F. Additional Experimental Results

In this section, we provide the complete experimental results for the prediction error (see Appendix F.1), and the average reward (see Appendix F.2) for all five test agents across the three benchmark environments. Further, we provide additional visualizations for the agent latent factors in Appendix F.3. We again emphasize that the additional results are consistent with the overall conclusions indicated in Section 6.

F.1. Detailed Prediction Error Results

In this section, we provide additional results for the prediction error experiments. As detailed in Section 6, we evaluate the accuracy of the learned transition dynamics for each of the five test agent, focusing on long-horizon model prediction. Specifically, we predict the next 50-step state trajectory given an initial state and an unseen sequence of 50 actions. The sequence of 50 actions are chosen according to an unseen test policy. Precisely, the test policies are fitted via DQN for MountainCar and CartPole, and via TD3 for and HalfCheetah, for the agent with the default covariate parameters. The test policies were trained to achieve an average rewards of -150, 150, 4000 for the MountainCar, CartPole, and HalfCheetah environments, respectively. As described in Section 6, we report the mean RMSE and the median R^2 across 200 trials. The results are summarized in Tables 9, 10, and 11 for MountainCar, CartPole, and HalfCheetah, respectively. Additionally, Figure 4 visualizes the prediction accuracy of PerSim up to 100-steps ahead predictions for two test agents in MountainCar and CartPole.

Table 9. Prediction Error: MountainCar

Data	Method	Agent 1 0.0001	Agent 2 0.0005	Agent 3 0.001	Agent 4 0.0025	Agent 5 0.0035
Pure	PerSim	0.025 (0.995)	0.023 (0.998)	0.048 (0.999)	0.015(0.984)	0.028 (0.939)
	Vanilla CaDM	0.709 (-3.326)	0.705 (-2.525)	0.668 (-2.05)	0.155 (-0.824)	0.142 (-1.391)
	PE-TS CaDM	0.789 (-4.203)	0.659 (-5.119)	0.487 (-6.758)	0.440 (-8.849)	0.438 (-11.438)
Random	PerSim	0.001 (1.000)	0.001 (1.000)	0.001 (1.000)	0.001 (1.000)	0.001 (1.000)
	Vanilla CaDM	0.731 (-4.673)	0.679 (-2.739)	0.647 (-2.054)	0.165 (-0.581)	0.143 (-0.940)
	PE-TS CaDM	0.792 (-4.380)	0.619 (-4.936)	0.387 (-3.941)	0.323 (-4.253)	0.316 (-4.845)
Pure- ϵ -20	PerSim	0.008 (0.998)	0.005 (0.999)	0.002 (1.000)	0.003 (0.999)	0.004 (0.998)
	Vanilla CaDM	0.696 (-3.420)	0.67 (-2.491)	0.638 (-2.054)	0.160 (-0.721)	0.144 (-1.295)
	PE-TS CaDM	0.791 (-4.294)	0.630 (-5.012)	0.410 (-5.056)	0.357 (-5.846)	0.353 (-6.691)
Pure- ϵ -40	PerSim	0.007 (0.998)	0.006 (0.999)	0.003 (1.000)	0.002 (1.000)	0.001 (1.000)
	Vanilla CaDM	0.619 (-3.558)	0.568 (-2.360)	0.546 (-1.430)	0.155 (-0.619)	0.144 (-1.174)
	PE-TS CaDM	0.780 (-4.312)	0.616 (-5.525)	0.409 (-5.277)	0.366 (-6.443)	0.363 (-7.580)

Table 10. Prediction Error: CartPole

Data	Method	Agent 1 (2/0.5)	Agent 2 (10.0/0.5)	Agent 3 (18.0/0.5)	Agent 4 (10/0.85)	Agent 5 (10/0.15)
Pure	PerSim	0.003 (1.000)	0.009 (0.999)	0.008 (1.000)	0.003 (1.000)	0.080 (0.994)
	Vanilla CaDM	3.190 (-0.698)	7.805 (-1.725)	11.091 (-1.624)	6.712 (-1.682)	12.31 (-1.953)
	PE-TS CaDM	2.940 (-7.009)	7.166 (-1.874)	9.769 (-1.742)	5.933 (-1.738)	12.24 (-2.207)
Random	PerSim	0.070 (0.683)	0.154 (0.868)	0.463 (0.229)	0.136 (0.964)	1.143 (-0.607)
	Vanilla CaDM	3.414 (-1.847)	5.973 (-2.090)	7.335 (-2.685)	4.351 (-1.997)	10.76 (-2.126)
	PE-TS CaDM	1.976 (-12.44)	3.744 (-1.772)	5.241 (-1.830)	2.043 (-2.620)	10.32 (-2.183)
Pure- ϵ -20	PerSim	0.004 (1.000)	0.010 (0.998)	0.011 (0.999)	0.004 (1.000)	0.170 (0.993)
	Vanilla CaDM	1.443 (-3.972)	4.078 (-0.851)	4.819 (-1.221)	2.614 (-0.789)	8.860 (-1.027)
	PE-TS CaDM	2.738 (-7.436)	6.997 (-1.978)	9.441 (-1.872)	5.618 (-1.780)	12.11 (-2.200)
Pure- ϵ -40	PerSim	0.008 (0.999)	0.009 (1.000)	0.007 (1.000)	0.015 (0.998)	0.232 (0.922)
	Vanilla CaDM	1.792 (21.912)	2.654 (-5.224)	2.618 (-4.390)	0.924 (-6.017)	8.848 (-2.685)
	PE-TS CaDM	2.795 (-6.400)	7.111 (-2.097)	9.576 (-2.049)	5.659 (-1.925)	12.28 (-2.418)

Table 11. Prediction Error: HalfCheetah

Data	Method	Agent 1 (0.3/1.7)	Agent 2 (1.7/0.3)	Agent 3 (0.3/0.3)	Agent 4 (1.7/1.7)	Agent 5 (1.0/1.0)
Pure	PerSim	1.258 (0.924)	5.303 (0.339)	5.830 (0.701)	1.357 (0.831)	2.582 (0.747)
	Vanilla CaDM	114.0 (-2.354)	108.1 (-1.264)	119.4 (-0.535)	121.9 (-1.743)	114.7 (-1.879)
	PE-TS CaDM	128.7 (-12.03)	132.1 (-8.116)	130.3 (-5.035)	129.0 (-11.26)	128.2 (-13.33)
Random	PerSim	1.419 (0.921)	4.758 (0.451)	6.917 (0.759)	1.374 (0.812)	2.683 (0.729)
	Vanilla CaDM	75.15 (-1.424)	74.14 (-0.726)	80.62 (-0.339)	78.60 (-1.423)	75.11 (-1.019)
	PE-TS CaDM	83.68 (-8.292)	86.23 (-5.076)	86.35 (-3.070)	84.01 (-6.994)	83.81 (-8.434)
Pure- ϵ -20	PerSim	1.318 (0.930)	4.880 (0.432)	4.792 (0.782)	1.321 (0.827)	2.451 (0.776)
	Vanilla CaDM	74.69 (-1.884)	76.63 (-0.897)	80.89 (-0.457)	81.66 (-1.556)	78.41 (-1.245)
	PE-TS CaDM	93.20 (-9.709)	96.10 (-6.053)	95.67 (-3.560)	94.04 (-8.057)	93.50 (-9.336)
Pure- ϵ -40	PerSim	1.274 (0.929)	4.719 (0.457)	4.410 (0.779)	1.249 (0.873)	2.452 (0.769)
	Vanilla CaDM	78.89 (-1.907)	80.55 (-0.929)	82.72 (-0.458)	81.66 (-1.501)	82.172 (-1.387)
	PE-TS CaDM	89.44 (-9.083)	92.14 (-5.461)	91.78 (-3.205)	90.47 (-7.779)	89.65 (-8.588)

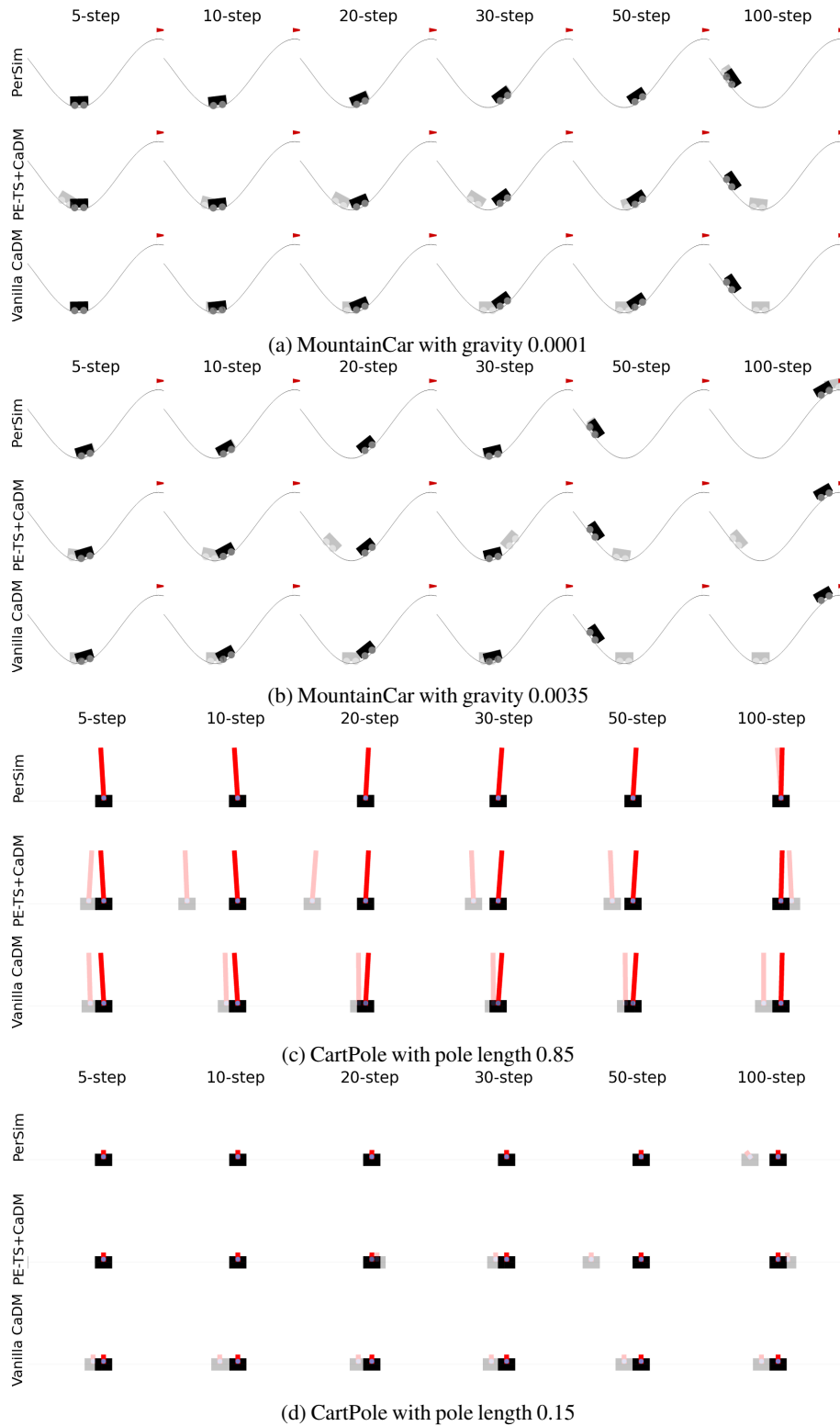


Figure 4. Visualization of the prediction accuracy of PerSim for two heterogeneous agents in MountainCar and CartPole, and how it compares with the two CaDM variants. Specifically, given an initial state and a sequence of actions, we predict future states for the next 100 steps. Ground-truth states and predicted states are denoted by the opaque and translucent objects, respectively.

F.2. Detailed Average Reward Results

In this section, we show the full results for the experiments for the reward achieved in each environment. Specifically, we report the average reward achieved by PerSim and several state-of-the-art model-based and model-free offline RL methods on the three benchmark environments across 5 trials. We evaluate the performance of each method using the average reward over 20 episodes for the model-based methods and the average reward over 100 episodes for the model-free methods. We repeat each experiment five times and report the mean and standard deviation.

The results are summarized in Tables 12, 13, and 14 for MountainCar, CartPole, and HalfCheetah, respectively.

Table 12. Average Reward: MountainCar

Data	Method	Agent 1 0.0001	Agent 2 0.0005	Agent 3 0.001	Agent 4 0.0025	Agent 5 0.0035
Pure	PerSim	-53.35± 2.55	-61.22± 4.53	-83.53± 7.95	-191.81± 4.44	-213.1± 3.59
	Vanilla CaDM	-87.60± 3.75	-258.2± 134	-482.4± 19.8	-500.0± 0.00	-500.0± 0.00
	PE-TS CaDM	-79.27± 2.72	-255.9± 102	-480.7± 19.0	-500.0± 0.00	-500.0± 0.00
	BCQ-P	-67.60± 22.3	-68.60± 19.6	-79.20± 14.7	-267.8± 202	-295.1± 180
	BCQ-A	-44.79± 0.08	-50.50± 0.40	-63.52± 0.19	-380.7± 170	-500.0± 0.00
Random	PerSim	-53.66± 0.75	-68.40± 1.58	-112.9± 4.50	-198.8± 6.77	-198.7± 24.2
	Vanilla CaDM	-85.73± 11.8	-242.8± 156	-494.7± 9.24	-500.0± 0.00	-500.0± 0.00
	PE-TS CaDM	-156.6± 3.05	-482.1± 13.8	-500.0± 0.00	-500.0± 0.00	-500.0± 0.00
	BCQ-P	-500.0± 0.00	-500.0± 0.00	-500.0± 0.00	-500.0± 0.00	-500.0± 0.00
	BCQ-A	-500.0± 0.00	-500.0± 0.00	-500.0± 0.00	-500.0± 0.00	-500.0± 0.00
Pure- ϵ -20	PerSim	-48.75± 3.64	-56.35± 6.82	-75.41± 14.1	-198.1± 7.11	-200.2± 23.45
	Vanilla CaDM	-81.53± 3.74	-296.0± 121	-475.1± 22.7	-500.0± 0.00	-500.0± 0.00
	PE-TS CaDM	-86.80± 4.11	-199.0± 39.9	-495.4± 3.98	-500.0± 0.00	-500.0± 0.00
	BCQ-P	-71.21± 24.4	-72.10± 20.5	-78.41± 14.3	-286.6± 196	-328.3± 158
	BCQ-A	-364.5± 180	-435.7± 63.7	-282.7± 308	-260.6± 51.4	-204.5± 68.9
Pure- ϵ -40	PerSim	-48.60± 2.83	-56.01± 6.06	-78.96± 16.0	-198.7± 4.58	-202.7± 21.0
	Vanilla CaDM	-80.70± 2.52	-202.8± 86.0	-499.1± 1.56	-500.0± 0.00	-500.0± 0.00
	PE-TS CaDM	-86.23± 4.11	-387.8± 14.1	-499.9± 0.06	-500.0± 0.00	-500.0± 0.00
	BCQ-P	-50.01± 7.50	-57.10± 10.3	-66.11± 3.91	-373.6± 180	-352.0± 211
	BCQ-A	-94.87± 0.88	-80.03± 38.5	-329.6± 242	-358.7± 201	-486.5± 20.6
	True env+MPC	-53.95± 4.10	-72.43± 7.80	-110.8± 23.8	-182.9± 22.9	-197.5± 20.7

Table 13. Average Reward: CartPole

Data	Method	Agent 1 (2/0.5)	Agent 2 (10.0/0.5)	Agent 3 (18.0/0.5)	Agent 4 (10/0.85)	Agent 5 (10/0.15)
Pure	PerSim	194.2± 3.23	189.8± 3.68	190.8± 4.12	186.3± 3.97	195.3± 2.10
	Vanilla CaDM	37.83± 2.37	17.92± 2.48	12.47± 0.49	23.74± 4.53	7.900± 1.31
	PE-TS CaDM	34.17± 1.14	17.60± 0.22	12.10± 0.96	22.64± 2.06	8.700± 0.58
	BCQ-P	166.2± 39.3	187.4± 14.7	187.2± 15.0	181.2± 13.5	182.8± 15.0
	BCQ-A	65.40± 67.5	138.0± 80.3	79.20± 79.9	79.20± 69.5	132.1± 85.0
Random	PerSim	178.4± 6.68	155.1± 14.4	175.9± 9.19	175.9± 7.34	119.1± 21.0
	Vanilla CaDM	35.10± 1.64	16.08± 0.48	11.37± 0.98	24.67± 4.70	8.550± 0.81
	PE-TS CaDM	33.03± 1.09	17.90± 0.93	10.94± 0.35	23.49± 2.60	9.920± 1.22
	BCQ-P	44.80± 34.0	58.21± 58.0	56.92± 56.0	57.91± 53.0	36.40± 36.0
	BCQ-A	43.90± 16.4	18.70± 13.1	7.200± 0.84	21.10± 5.81	39.50± 12.1
Pure- ϵ -20	PerSim	190.82± 1.63	189.4± 5.41	189.3± 4.72	184.4± 7.20	195.1± 3.20
	Vanilla CaDM	37.53± 2.07	16.94± 1.61	13.33± 0.68	22.10± 1.49	8.300± 0.79
	PE-TS CaDM	38.39± 4.23	17.55± 2.37	13.60± 2.34	24.81± 3.48	8.670± 0.37
	BCQ-P	98.90± 30.2	170.9± 19.0	163.0± 36.5	162.1± 15.5	86.10± 72.1
	BCQ-A	67.30± 62.2	130.0± 76.1	33.40± 0.62	65.60± 51.8	140.0± 80.6
Pure- ϵ -40	PerSim	183.7± 10.5	173.4± 10.8	184.8± 3.79	173.3± 5.50	195.9± 4.61
	Vanilla CaDM	36.46± 2.52	16.41± 0.92	14.50± 1.98	23.64± 1.54	8.390± 1.29
	PE-TS CaDM	40.47± 1.52	19.00± 2.39	12.87± 1.41	22.45± 2.20	8.800± 1.23
	BCQ-P	28.90± 6.80	24.97± 12.8	27.90± 25.9	31.80± 25.9	18.50± 11.1
	BCQ-A	34.60± 1.55	23.20± 17.8	7.180± 0.76	47.71± 48.7	23.20± 9.44
	True env+MPC	198.9± 3.80	191.2± 21.0	194.8± 14.2	188± 23.0	199.1± 2.80

Table 14. Average Reward: HalfCheetah

Data	Method	Agent 1 (0.3/1.7)	Agent 2 (1.7/0.3)	Agent 3 (0.3/0.3)	Agent 4 (1.7/1.7)	Agent 5 (1.0/1.0)
Pure	PerSim	378.5±124	275.3±118	612.4±261	42.02±26.9	950.1±336
	Vanilla CaDM	-346.5±162	-270.0±25.7	-306.0±87.6	-284.3±83.7	-263.7±113
	PE-TS CaDM	-405.8±32.6	-251.8±107	-380.5±160	-255.8±48.3	-234.6±65.7
	BCQ-P	549.8±322	2005.9±152	-65.18±92.8	2564.1±70.2	2469.8±67.2
	BCQ-A	-262.7±96.6	-139.0±236	165.6±83.1	1649.0±622	937.2±221
Random	PerSim	586.4±121	352.7±480	157.1±463	616.6±16.2	207.6±95.0
	Vanilla CaDM	-271.8±210	-135.5±150.5	-223.2±143	-196.0±72.0	-154.9±83.9
	PE-TS CaDM	-197.7±27.6	-112.4±31.4	-133.5±22.4	-111.5±28.0	-115.9±27.2
	BCQ-P	-1.460±0.16	-1.750±0.22	-1.690±0.19	-1.790±0.21	-1.720±0.20
	BCQ-A	279.6±160	-44.05±24.9	-75.03±44.0	-109.8±11.1	-217.5±60.0
Pure- ϵ -20	PerSim	827.8±353	617.7±270	464.0±377	495.1±17.2	490.6±121
	Vanilla CaDM	-120.1±29.3	-96.10±53.9	-138.4±127	-90.40±70.4	-88.25±62.7
	PE-TS CaDM	-401.3±10.5	-346.5±58.7	-323.1±86.7	-323.1±49.5	-308.7±94.7
	BCQ-P	254.6±351.	406.7±71.1	385.9±57.1	-95.34±65.8	738.0±512
	BCQ-A	376.8±102	84.66±53.3	230.1±10.0	1180.8±87.3	617.5±32.6
Pure- ϵ -40	PerSim	477.7±36.0	781.5±130	769.8±114	610.4±33.8	934.7±36.7
	Vanilla CaDM	-276.5±50.5	-239.7±70.7	-302.3±44.1	-207.3±107	-196.1±108
	PE-TS CaDM	-198.9±68.7	-180.0±33.4	-194.6±21.0	-82.81±1.42	-181.5±21.2
	BCQ-P	78.25±199	173.8±189	417.1±155	-56.12±64.4	55.46±128
	BCQ-A	269.2±60.7	-181.5±57.4	193.0±31.8	636.4±137	207.0±105
	True env+MPC	7459±171	42893±6959	66675±9364	1746±624	36344±7924

F.3. Visualization of Agent Latent Factors

In this section, we visualize the learned agent latent factors associated with the 500 heterogeneous agents in each of the three benchmark environments. Specifically, we visualize the agent latent factors in MountainCar, as we vary the gravity (Figure 5a); CartPole, as we vary the pole’s length and the push force (Figures 5c and 5b, respectively); HalfCheetah, as we vary the cheetah’s mass and the joints’ damping (Figures 5e and 5d, respectively).

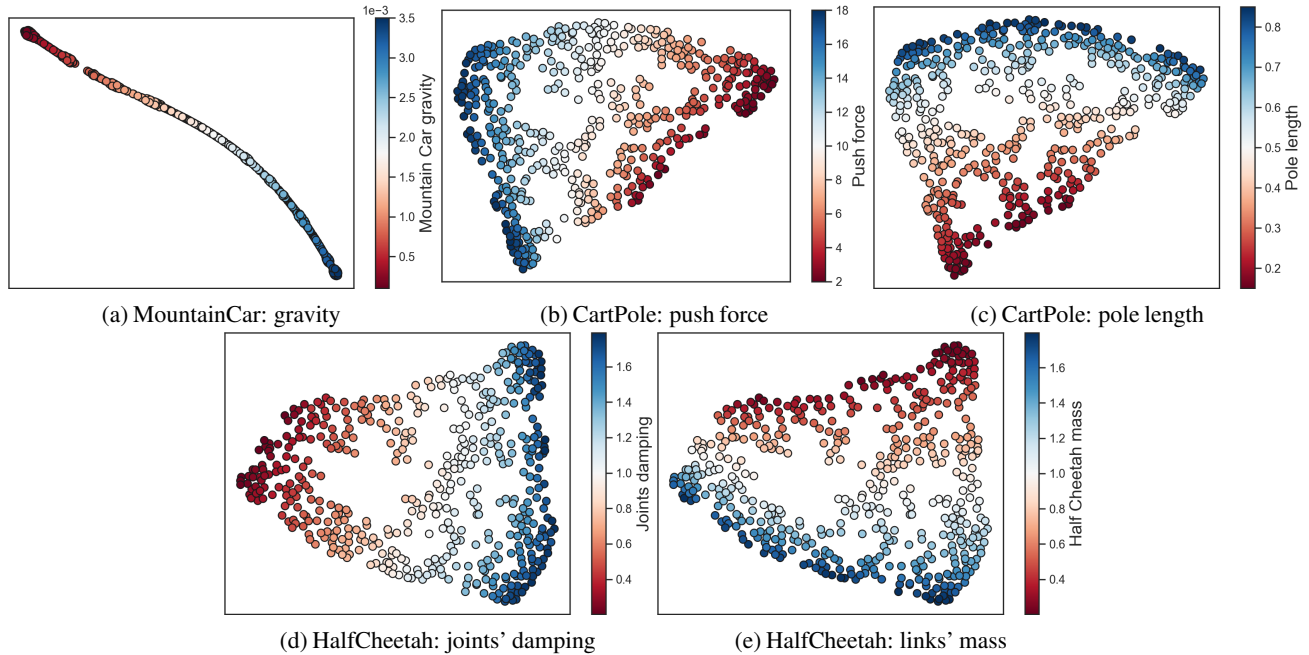


Figure 5. t-SNE (Van der Maaten & Hinton, 2008) visualization of the agent latent factors for the 500 heterogeneous agents in MountainCar, CartPole, and HalfCheetah. Colors indicate the value of the modified parameter in each environment (e.g., gravity in MountainCar). These figures demonstrate that the learned latent factors indeed capture the relevant information about the agents heterogeneity in all environments.